STUDY ON ORGANIC MATTER ENRICHMENT AND PRESERVATION CONTROL IN CARBONATE SOURCE ROCK: FIELD ANALOGUE FROM THE MESOZOIC SEDIMENTARY ROCK IN SOUTHEAST-ARM OF SULAWESI

炭酸塩岩根源岩における有機物の濃集と保存に関する研究：インドネシア・スラウェシ島南東部中生界堆積岩の場合

MUHAMMAD SULHUZAIR BURHANUDDIN

ムハンマド　シュルフルザイル　ブルハヌッディン

DOCTORAL THESIS

Submitted in fulllment of the requirements for the Degree of Doctor of Science

Department of Goesciences, Geotechnology, Material Engineering for Resources
Faculty of International Resources Sciences
Akita University

AKITA, JAPAN
August, 2024

ABSTRACT

While carbonate rock is often attributed as an excellent reservoir due to its favorable porosity and permeability, such lithology also has a crucial role in the generation subsystem to act as

source rock. However, detailed lithological and petrochemical characteristics, together with tectono-sedimentation controls on the deposition and organic matter enrichment of carbonate source rocks, are still poorly documented. Hence, this study focused on understanding the organic matter enrichment and preservation controls of carbonate source rock. Southeast arm of Sulawesi, is one of the frontier areas in eastern Indonesia that provides excellent records for such studies because Mesozoic carbonate intervals, the Triassic-Jurassic Tokala and Cretaceous Matano Formations, cropped out widely on the surface together with hydrocarbon manifestations. Both megascopic and microscopic observations were combined with comprehensive inorganic and organic geochemistry analyses to unravel control of the enrichment and preservation of organic matter preservation in carbonate source rock. Due to the high deformation and complexity of lithofacies determination, major elements representing mudstone dominant constituents were used to classify the lithology into “mixed” shales, argillaceous shale, and argillaceous mudstone. To summarize, we provide excellent evidence that the global “carbonate source rock” term is applied to our “mixed” shale, composed of mixed carbonate and siliciclastic materials. The equilibrium of these constituents is further related to two critical aspects in our novel proposed model, which are tectonic and sedimentological aspects, especially detrital input and carbonate development. From the model, organic matter accumulation occurred in the basin margin (Bule “mixed” shale facies) with a suspension mechanism and the latter was preserved under the anoxic bottom of water. Moreover, fault activities during the rifting event triggered mass transportation to the fore slope (Wiwi “mixed” shale facies) resulting in rapid sedimentation which exhibits good organic matter preservation. This new model re-updated the understanding of global “carbonate source rock” and though applicable for other regional and global syn-extensional carbonate source rock.

ACKNOWLEDGEMENTS

I express my sincere gratitude to people who have helped me to finish this dissertation. Firstly, I owe my gratitude to my supervisors, Professor Shun Chiyonobu and Dr. Takuto Ando, who patiently provided materials, supervision and direction with the project, and constantly stimulated my interest throughout my research.

I am very grateful to my best friends, Mr. Barry Majeed Hartono and Dr. Sc. Paolo Martizzi with whom I have discussed about my research, and helped me during finishing my publication.
I would like to acknowledge my fellow Petroleum Geology Laboratory member Mr. Takumi Mimura and the other PGL members for all help and support during my research in Akita University and helped me a lot when I first arrived in Akita.
I am very grateful also to Indonesian Student Association member and all the friends from Akita University, that supported me whenever I need.
I am grateful for all the support provided by acquaintances in Indonesia (Mrs. Anggi Yusriani, Dr. Sc. Renaldi Suhendra, Dr. Sc. Muh. Andriansyah Gurusinga, Mr. Suryawan Asfar, Dr. Ratna Husain L., Dr. Eng. Meutia Farida, Mr. Baso Rezki Maulana), as despite any separation in location, they consistently offered an empathetic ear and encouragement through all stages.
I would like to thank all the Professors, Researchers, and Staff from Akita University that constantly help international students during their life in university.
Lastly, I deeply dedicate this thesis to my family especially to in memoriam my beloved father Drs. Burhanuddin for all the motivation and strength, and to my lovely mother Sitti Syahriati, my wife Nur Hanifah Muchtar, my daughter Sitti Syafiah Yumna Sulhuzair and Sitti Tsania Alawiyah Sulhuzair, for always love me in any situation. My brother and sisters Muhammad Basith, Yuniarti Ekasaputri, and Ainun Mardiah, my mother Hj. Nur Aeni Kasim and father H. Muchtar Pasarai, who always give strength and motivation.
This work was supported by the Ministry of Education, Culture, Sports, Science and Technology (MEXT) Doctorate Scholarship, obtained through the precious support of Akita University.

LIST OF CONTENTS

Chapter I: INTRODUCTION

I.1 Research background, aims and datasets

Carbonate rocks have been long understood to be the main target of hydrocarbon exploration as such lithology exhibits good porosity and permeability to act as a reservoir (secondary porosity; North, 1990; Allen and Allen, 2013; Selley and Sonnenberg, 2015). Current understanding pointed out that carbonate rocks have been also proven to act as "hydrocarbon kitchen" in several global super basins, e.g., Jurassic Sargelu Formation (Middle East; Hakimi and Najaf, 2016), Jurassic Smackover Formation (Gulf Coast; Oehler, 1984), and Cretaceous La Luna Formation (Latin America; Zumberge, 1984). Such phenomenon has attracted numerous researchers to study carbonate source rocks, in which most studies focused on discriminating between carbonate and clastic source rocks based on their organic content (Hunt, 1996; Xia et al., 2019), paleo-environment of carbonate source rocks (Palacas et al., 1984), and carbonate-derived oil characteristics (Hughes, 1984; Zumberge, 1984; Subroto et al., 1991). Detailed lithological and petrochemical characteristics, together with tectono-sedimentation controls on the deposition and organic matter enrichment of carbonate source rocks, however, are still poorly understood.

In this thesis, the depositional and organic matter enrichment mechanism on carbonate source rock were emphasized which is also considered tectonic event. We comprehensively combined conventional approaches, such as field geological observation and petrography analysis, with detailed inorganic and organic geochemistry analyses from the Pre-Tertiary carbonate interval cropped out in Southeast Sulawesi, eastern Indonesia to unravel these carbonate intervals characterization. These Pre-Tertiary carbonates were selected for this study as similar Pre-Tertiary carbonate intervals in neighboring productive basins, such as Seram (Price et al., 1987; Peters et al., 1999; Noble et al., 2009; Hartono et al., 2021, 2023) and Buton Basins (Davidson, 1991; Tobing, 2008; Satyana et al., 2013), have been proven to act as hydrocarbon source rocks. Indeed, compared to other basins in eastern Indonesia, exploration was scarce in our research area. However, numerous hydrocarbon manifestations have been reported (Kurniawan et al., 2019; Burhanuddin et al., 2021), suggesting that the generation subsystem was active, while no commercial hydrocarbon accumulation was probably related to the lack of understanding of the petroleum system elements in the research area. In addition, the carbonate interval cropped out in Southeast Sulawesi displays excellent facies variation, which is suitable for this study. Hence, the origin of carbonate source rocks could be understood for further conventional and unconventional exploration, not restricted to regional areas, but also in global basins with carbonate source rocks.

Chapter II: GEOLOGICAL SETTING

Sulawesi Island is divided into four tectonic provinces (Surono and Hartono, 2013) separated by complex structures from the west to the east, respectively, magmatic arc, central metamorphic block, ophiolite belt, and Australian-derived microcontinent. The border between each tectonic province, however, is still unclear, for example, some Pre-Tertiary sedimentary rocks occurred as small blocks in the ophiolite belt province. Our research area is situated in the southeast arm of Sulawesi, in which part of the microcontinent bounded by two major strike-slip faults, the Matano Fault in the north and the Lawanopo Fault in the southern part of the research area (Figure 1, Rusmana et al., 1993; Surono and Hartono, 1993; Nugraha and Hall, 2022).

The southeast arm of Sulawesi is formed by multiple tectonic stages, from the break-up of Gondwana to the collision of microcontinent in the margin of Sundaland, resulting in complex Pre-Tertiary to Tertiary stratigraphic variations (Figure 2: Rusmana et al., 1993; Simandjuntak et al., 1993; Surono and Hartono, 1993; Surono, 1994, 1998; Spakman and Hall, 2010; Rudyawan and Hall, 2012; Nugraha and Hall, 2022). The SE Sulawesi fragment (term from Advokaat and Hinsbergen, 2023) rifted from Gondwana (West Australia) during the Early Permian(?)-Triassic. During the syn-rift stage, basin filling was dominated by the deposition of terrestrial to fluvio-deltaic sediments represented by the Meluhu Formation. Later, marine incursion resulted in carbonate development in the basinal area, while the siliciclastic deposition still continued in the west (Figure 2; Surono and Hartono, 2013). This carbonate interval is referred to as Tokala Formation (Rusmana et al., 1993; Villeneuve et al., 2001; Surono and Bachri, 2002; Surono and Hartono, 2013) deposited in the carbonate platform with various facies from intertidal facies to carbonate reef. Surono and Hartono (2013) observed that the carbonate reef was drowned due to rapid subsidence in the upper part. This Triassic-Jurassic carbonate could be correlated with other carbonates in eastern Indonesia, such as Manusela and Saman-Saman Formations in Seram Basin (Audley-Charles et al., 1979; Kemp and Mogg, 1992) and Winto Formation in Buton Basin (Davidson, 1991; Surono and Hartono, 2013). The rifting continues until the break-up event marked by regional unconformable boundaries as a result of major uplift. After the break-up event, a north-oriented drifting of the microcontinent occurred from the Cretaceous through the Early Cenozoic. In this drifting stage, the basin was far from the sediment source, resulting in dominant carbonate deposition, which is represented by two carbonate formations, the Cretaceous Matano and Paleogene Tampakura Formations (Figure 2; Rusmana et al., 1993; Surono and Bachri, 2002; Surono and Hartono, 2013, Nugraha and Hall, 2022). Several researchers (Surono and Hartono, 2013; Nugraha and Hall, 2022) noted an unconformity boundary between these two carbonate intervals that might

be related to a deepening event. Specific to the Matano Formation, the carbonate was deposited in the shallow to deep marine environment during the major transgressive event (Simandjuntak, 1991, 1997; Rusmana et al., 1993; Surono and Hatono, 2013; Nugraha and Hall, 2022).

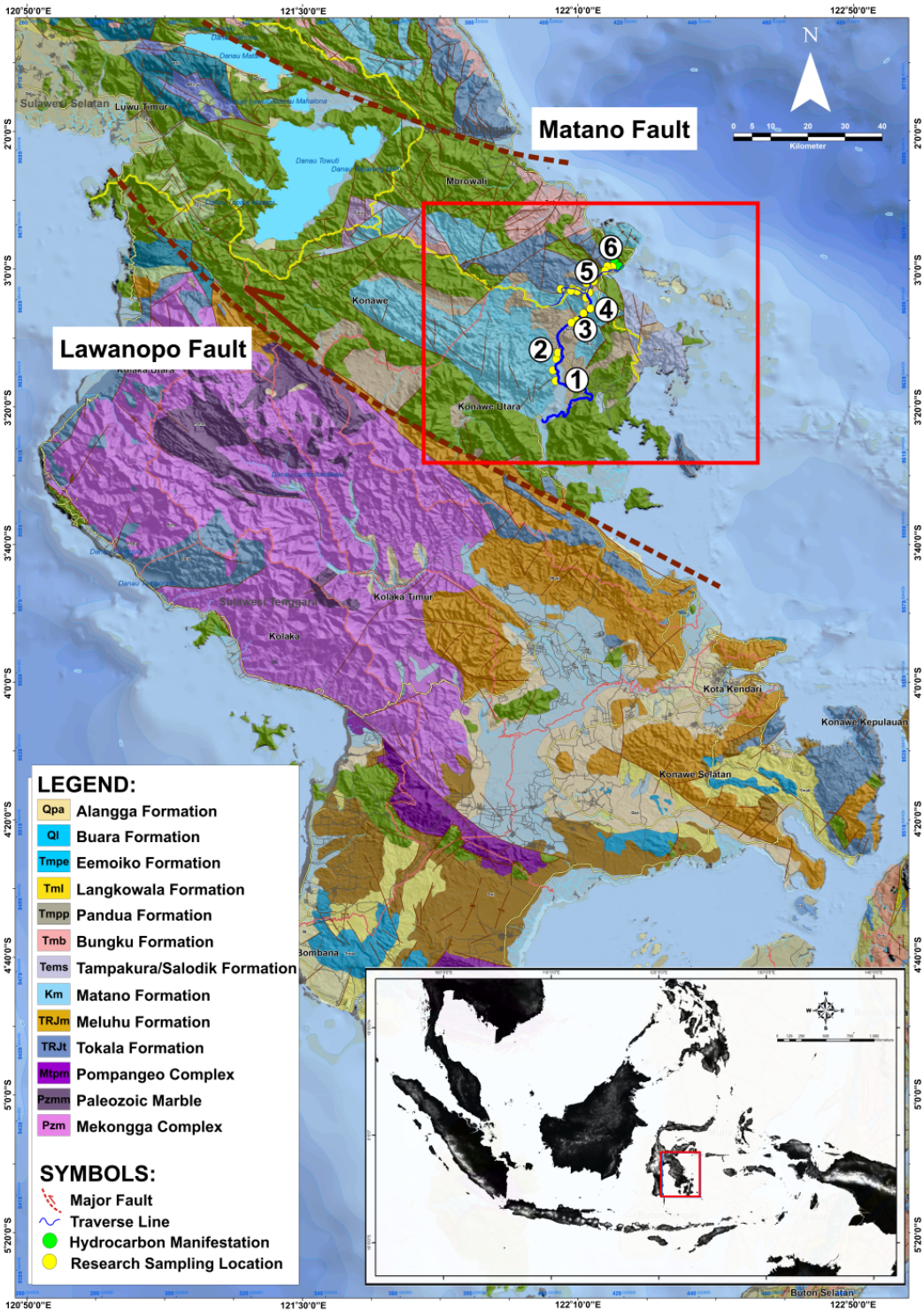

Figure 1. Regional geological map of Southeast-arm of Sulawesi (adapted from Rusmana et al., 1993; Nugraha et al., 2022), in which our research area is marked by the red square. Geological surveys were focused on the Mesozoic carbonate interval. Hydrocarbon manifestation was also noted in the outcrops and sampled for further biomarker analysis.

The drifting period was terminated by the Early Miocene collision event of the Banggai-Sula microcontinent, resulting in the major uplift of the Pre-Tertiary interval that acted as the provenance of the latter deposition through Neogene. This deposition was controlled by the orogenic system represented by molasse sediments (syn-orogenic deposit), which were deposited in various environments from terrestrial to shelf environment (Figure 2; Nugraha and Hall, 2018, 2022; Nugraha et al., 2022). In the latter understanding, Nugraha and Hall (2022 and references therein) divided these syn- to post-orogenic deposits into the Early Miocene Bungku Formation, Late Miocene Pandua Formation, Miocene-Pleistocene Langkowala Formation, and Pliocene Eemoiko Formation. The youngest formations in the area are the Quaternary clastic Buara and carbonate Alangga Formations (Nugraha and Hall, 2022).

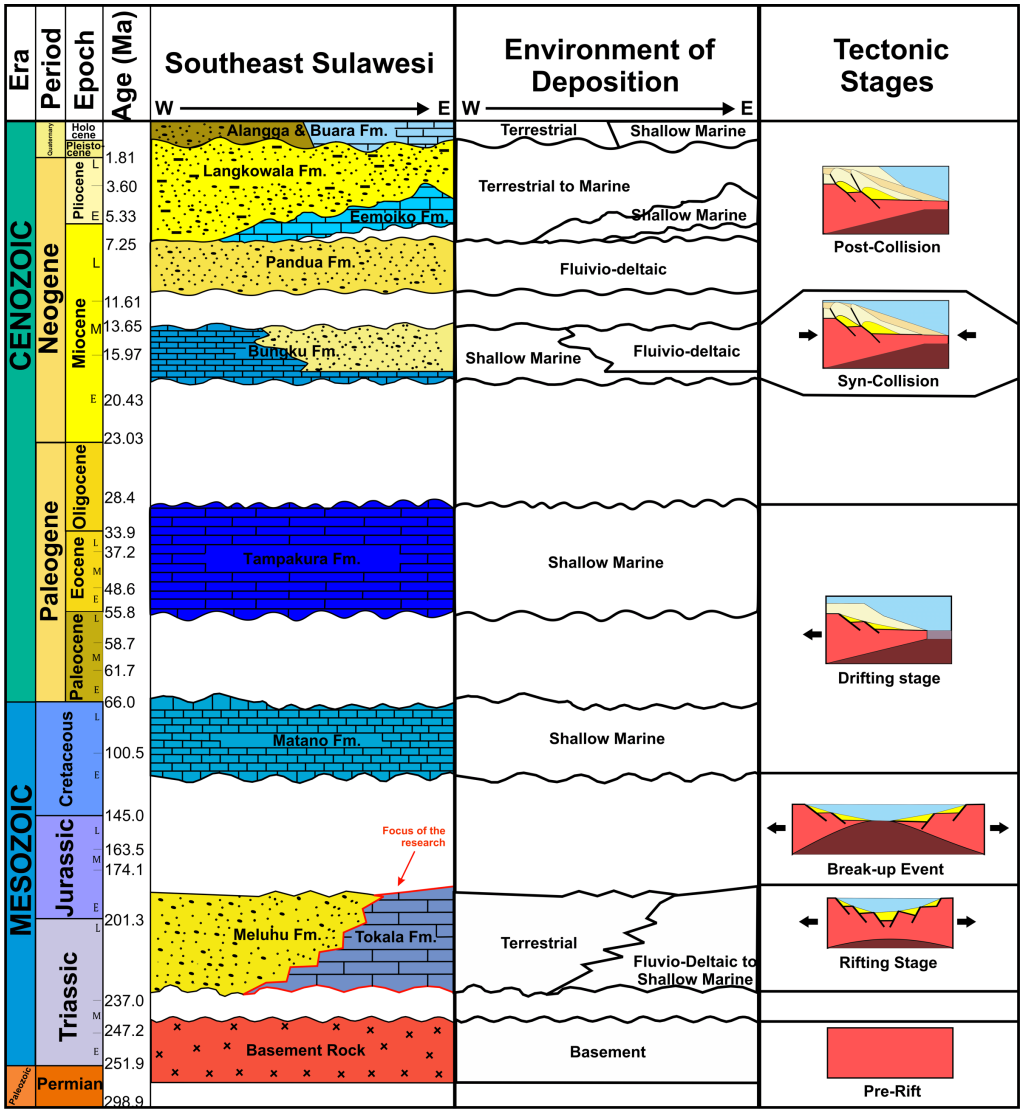

Figure 2. Regional tectonostratigraphy of Southeast-arm of Sulawesi with the depositional environment (modified from Rusmana et al., 1993 and Nugraha et al., 2022). This research focused on the Mesozoic carbonate intervals, which are the Triassic-Jurassic Tokala Formation (syn-rift deposit) and Cretaceous Matano Formation (syn-drift deposits) which are separated by a major unconformity.

Chapter III: MATERIALS AND METHODS

3.1 Field observation and sampling

The geological field observation was conducted in North Konawe and South Bungku, Southeast Sulawesi with seven stratigraphic sections from south to north (Figure 1), respectively, (1) Wiwi-1, (2) Wiwi-2, (3) Prasasti-1, (4) Prasasti-2, (5) Bule-1, and (6) Bule-2. Based on the previous survey from the Indonesia Geological Agency (Rusmana et al., 1993), lithologies traversed all sections belong to the Tokala Formation, while those in Prasasti-1 and Prasasti-2 sections are part of the Matano Formation. Neither age data was not available, nor biostratigraphic analysis was not the main focus of this study, the formations assignment was later validated with the correlation between lithological characteristics and regional lithostratigraphy (Rusmana et al., 1993; Surono and Hartono, 2013; Surono, 1994). A total of 92 rock samples were collected from shale and limestone cropped out along road-cuts. These samples are considered fresh as the outcrop was excavated at least 15 cm of thickness prior sampling. In addition, one sample with oil-stain was also acquired from limestone in the Bule-1 section (Section 6; Figure 1). To ensure proper preservation, all samples were stored in well-sealed plastic bags, while rock containing oil-stain were wrapped with aluminum foil to avoid contamination (Simmons, 2023).

3.2 Petrographic analysis

A total twenty-seven samples, consisting of nineteen representative shales from all sections and a total eight limestone selected from Wiwi-1, Wiwi-2, Bule-1, and Bule-2, respectively, were then selected for petrographic analysis to obtain detailed lithological descriptions. Prior to the preparation, mudstone and shale were hardened with epoxy solution (resin and catalyst) and left for 12 hours to avoid internal break-up as such lithology was too friable for primary cuttings. After primary cutting, shale and limestone chunks were polished, in order, from mesh #350, #800, #1000, #2000, #3000 and attached to slide glass. Secondary cutting was performed to thin attached samples into about 1-2 mm thick, and a prepalap cutter by Maruto Instrument, equivalent to #600 mesh powder, was utilized to grind thick blocks down to about 30 microns. Finally, samples were polished with powder sequentially from mesh #1000, #2000, #3000, to #6000. These petrographic slides underwent detailed observation under transmitted and reflective light employing a Nikon H600L microscope.

3.3 X-ray fluorescence analysis

Elemental composition was used for classifying our lithologies. Whole major oxides (SiO_2, TiO_2, Al_2O_3, Fe_2O_3, MnO, MgO, CaO, K_2O, and P_2O_5) and some trace elements (Ba, Cr, Cu, Nb, Ni, Pb, Rb, S, Sr, V, Y, Zn, Zr) were obtained from X-ray fluorescence (XRF) analysis. Twenty-seven representative samples from seven sections were subjected to this

analysis using Rigaku ZXS Primus II XRF instrument. Before analysis, pulverization was carried out to attain 5-6 grams of powder samples so that the powder became homogenous, after which they were carefully placed within the assigned pellet rings. Following this step, sample powders were compressed using a flat disk to obtain appropriate pellet samples (details about pellet preparation for XRF are available in Takahashi, 2015).

3.4 Bulk organic geochemistry

In this study, bulk-rock geochemistry was identified through TOC Rock-Eval analysis, a widely accepted and standardized method for evaluating the concentration of organic carbon and assessing hydrocarbon potential (Peters and Cassa, 1994; Lafargue et al., 1998). The measurement of organic matter quantity was conducted using the Rock-Eval IV Instrument, manufactured by Vinci Technologies, at both the laboratory of Akita University, Japan, and the Geoservices Laboratory in Indonesia. The Rock-Eval pyrolysis technique, following established methods, involved heating a predetermined amount of rock within an inert atmosphere (helium or nitrogen) using a temperature-programmed heating method (Lafargue et al., 1998).

This method yields several key parameters crucial for understanding the organic content and hydrocarbon potential of the samples, including hydrocarbon volatile content (S_1), hydrocarbon generation potential (S_2), the maximum temperature at which hydrocarbon compounds are released (T_{max}), and the quantity of organic carbon dioxide (S_3). Determination of total organic carbon (TOC) content is achieved through oxidation under air, with the remaining organic carbon (S_4) measured subsequent to the pyrolysis process (Lafargue et al., 1998). Additionally, the hydrogen index (HI) and oxygen index (OI) are determined using Rock-Eval analysis, contributing to the comprehensive evaluation of source rock potential in this research (Peters, 1986; Peters and Cassa, 1994; Lafargue et al., 1998; Behar et al., 2001; Martizzi,

A total 92 samples consisting of 60 shales, 10 mudstones, and 22 limestones were evaluated by employing the Rock-Eval 6 pyrolysis instrument manufactured by Vinci Technologies. These samples were grounded into 300-400 mesh sample powder (clay size), and later, 0.6 to 0.7 g fractions were inserted into designed crucibles for analysis. Details of the Rock-Eval pyrolysis technique are available in Lafargue et al. (1998) and Behar et al. (2001). Several parameters were acquired from this analysis, such as total organic carbon (TOC), S_1, S_2, S_3, and T_{max}.

3.5 Gas chromatography and gas chromatography-mass spectrometry

Samples with appropriate organic content (TOC > 0.5 %) were selected for further geochemical analysis using gas chromatography (GC) and gas chromatography-mass

spectrometry (GC-MS) to obtain detailed biomarker data. First, samples were extracted using the organic solvent methanol (MeOH) in a quantity of 20 ml, followed by a mixture of MeOH and dichloromethane (DCM) in a 1:1 ratio, and finally dichloromethane (DCM) in a volume of 20 ml (Sawada et al., 1996; Sawada, 2006; Ando et al., 2017a, 2017b; Ando et al., 2022). After the extraction process, fractionation was performed using silica gel and organic solvents such as hexane, toluene, ethyl-acetate (EtAc), and MeOH to separate the aliphatic and aromatic fractions. Subsequently, 1 µl of aliphatic and aromatic fractions were injected into a gas chromatograph Hewlett Packard 6890N and Agilent 5975 instrument, with a specification of the column used in the analysis are HP-PONA Methyl-Siloxane capillary column, 50 m x 0.2 mm i.d. x 0.5 µm film thickness, and H_2 carrier gas. The column was heated from 35^{o}C for 10 minutes, then heated to 320^{o}C for 60 minutes with a rate of 5^{o}C/minute.

Chapter IV: RESULTS

4.1 Lithological characteristics: from outcrop-scale to micro-scale

From the south section, the stratigraphic interval of Tokala Formation is indicated by the intercalation of limestone and shale with limestone beds predominating in the Wiwi-1 section (Figure 3). The limestone and shale are well-stratified with a sharp contact but occasionally undulated and erosional contacts were observed. This stratigraphic interval is overlain by Quaternary deposits, indicating subsequent geological events and sedimentary processes that have influenced the surface morphology (Figure 4A and 4B). Limestone displays a light gray color, matrix-supported, moderately sorted, intense bioturbated and massive, with a thickness for each layer ranging from 32 to 50 cm (Figure 4C-4E). Soft sedimentary structures, such as slump and convolute, were created by the limestone layer. Under microscopic observation, the limestone is composed of skeletal grain, mostly foraminifera followed by mollusk grains, in the micritic matrix, so the lithology is assigned to foraminifera wackestone (FW) facies (Figure 4F-4H). Foraminifera is diverse with various test shapes, such as elongated, oval, and circular shape (Figure 4G and 4H). Thin shale layers (5-12 cm) intercalated with wackestone, are composed of carbonate grain within argillaceous matrix, occasional carbonaceous layer, together with bitumen streaks that intersect the layer. Significant concentrations of amorphous organic matter (AOM) were observed together with woody OM (Figure 4I and 4J) dispersedly distributed in the matrix. Carbonate grain is dominantly composed of skeletal fragments derived from foraminifera and mollusk with a size of 0.15 to 1.1 mm. Compared to the limestone, skeletal grain in the shale layers tends to be homogenous. To note, almost all original structures of skeletal fragments were already destroyed by extensive diagenesis, specifically neomorphism, as large calcite crystals grew inside shells (Figure 4G, 4H, and 4J). Later, shale in the Wiwi-1 section is assigned as massive shale (MS) facies.

Another shale and limestone alternation of Tokala Formation was cropped out in the Wiwi-2 section, but different from the previous section, the alternation is dominated by shale and are overlain by quaternary deposits (Figure 3 and Figure 5A). The limestone is poorly stratified and clear contact between these lithologies is unclear as the layer tends to be discontinuous. Interestingly, soft sedimentary structure occurred not only as slump and convolute layer, but also in the form of another type, where limestone blocks are submerged in the underlain shale layers (Figure 5C, 5D, 5F, and 5G). Shales have a dark gray color and could be considered moderately bioturbated, poorly laminated based on field observations which tend to show weak (wavy-irregular sinuous) lamination which we interpreted as convolute part of the Buoma sequence (Figure 5F, 5G, 5J anad 5K).

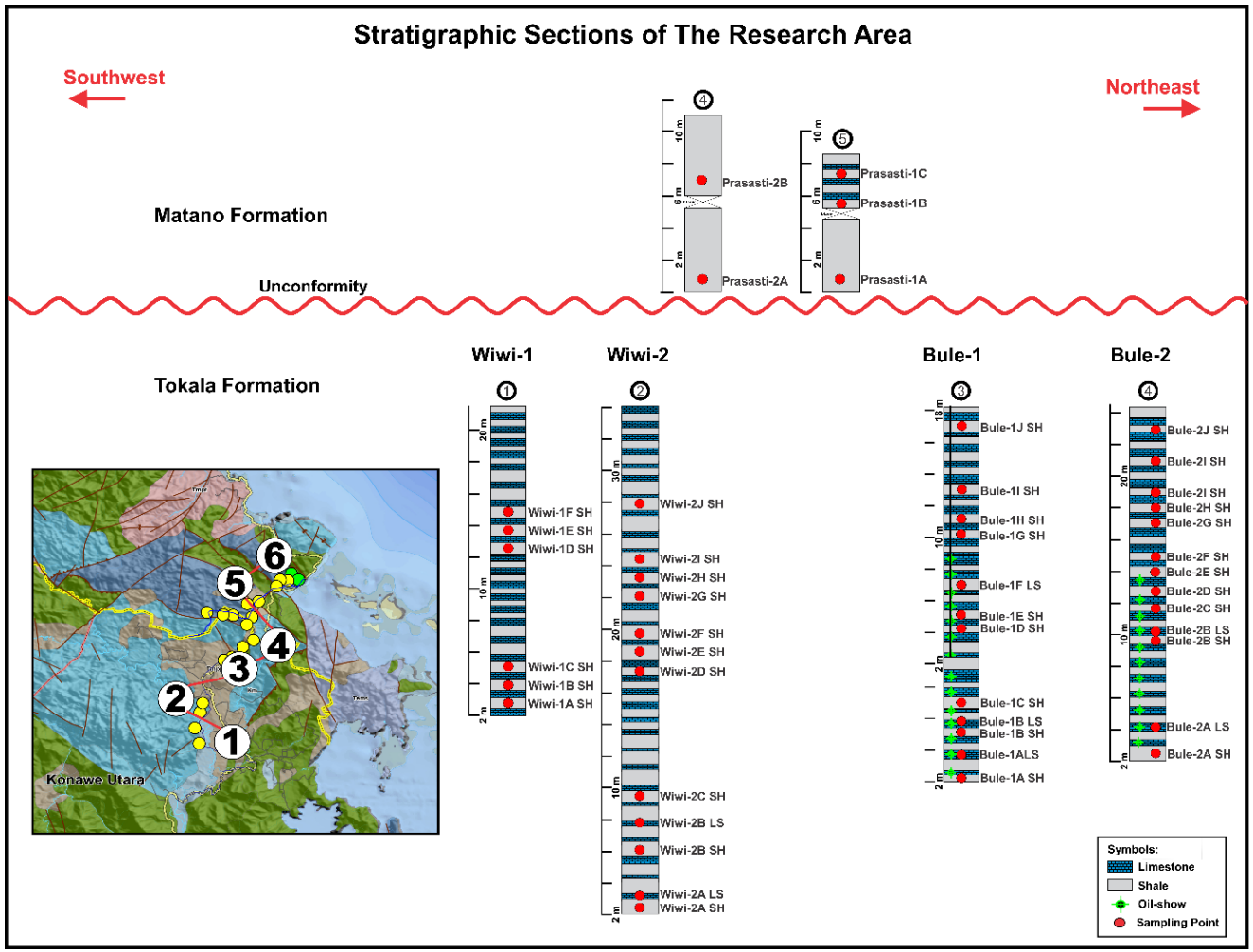

Figure 3. Stratigraphic succession of the traversed Triassic-Jurassic Tokala and Cretaceous Matano Shale (adapted from Rusmana et al., 1993; Surono and Bachri, 2002; Surono and Hartono). The stratigraphic section comprises six sections which are (1) Wiwi-1, (2) Wiwi-2, (3) Prasasti-1, (4) Prasasti-2, (5) Bule-1, and (6) Bule-2 that are distributed 116 km from south to north.

Organic matter tends to be more abundant compared to the Wiwi-1 MS facies but still with the same type, which is composed of AOM and woody OM (Figure 5I and 5J). This OM is distributed in both dispersed- and laminae-fashion (Figure 5H, 5J, and 5K). Moreover, framboidal pyrite is common and poorly sorted within the shale facies, dominantly composed of large-size framboids (10.7-17.5 μm), followed by moderate-size framboids (6-9 μm; Figure 5I – 5K). We assigned this shale as weakly laminated shale (WLS) facies. Additionally, shale layers have oil-odors, but oil-stain was not visible both in megascopic and microscopic observations. Limestone layers were also changed into finer grain, matrix-supported, and absences of skeletal fragments. Hence, limestone in this section represented lime mudstone (LM) facies.

Further north, another Tokala Formation interval attributed by 21-meter-thick outcrops comprised of good stratification of limestone and shale with equal thickness proportion were traversed in the Bule-1 and Bule-2 sections (Tokala Formation; Figure 3). Here, shale layers display similar characteristics with all aforementioned sections, but skeletal fragments were suspended between argillaceous matrix and organic-rich layers (Figure 5P). In addition, skeletal grains tend to be not diverse, compared to other shale facies, which are only composed of oval-shaped foraminifera that have already undergone neomorphism (Figure 6G, 6I, dan 6J). Moreover, foraminifera display similar orientations with the long axis perpendicular to the lamination (Figure 6G). In terms of organic matter, AOM was dominantly present creating laminae and OM network, while woody OM was scarce. Less prevalent framboidal pyrite was observed, with aggregate morphology exhibiting more finer framboids from 2.7-3.5 μm (Figure 6K). The shale intervals here are described as strongly laminated shale (SLS) facies where the interlayered limestone could be classified as FW facies but with lower concentration and diversity of skeletal fragments. Another interesting feature found in the section is the occurrence of veins filled with bitumen, probably related to hydrocarbon generation. Not just under the microscope, oil-bleed and strong oil odor were also noted within the fracture of overlain limestone in this section (Figure 6A-6C).

Another interval of the Tokala Formation was also discovered on the northeast side of the previous section, situated in the Torete area. This outcrop presents a similar lithological composition to the previous stratigraphic interval from the Bule-1 section (refer to Figure 7A). Comprising interbedded limestone and shale, this outcrop exhibits well-stratified shale layers alternating with limestone formations, with shale thickness ranging approximately from 20 to 30 cm, with visible fissile structures (see Figure 7B). Notably, the limestone layers observed during field investigations show an average thickness ranging between 20 to 35 cm, intriguingly, oil-bleed was also observed within this interval (Figure 7B-7D).

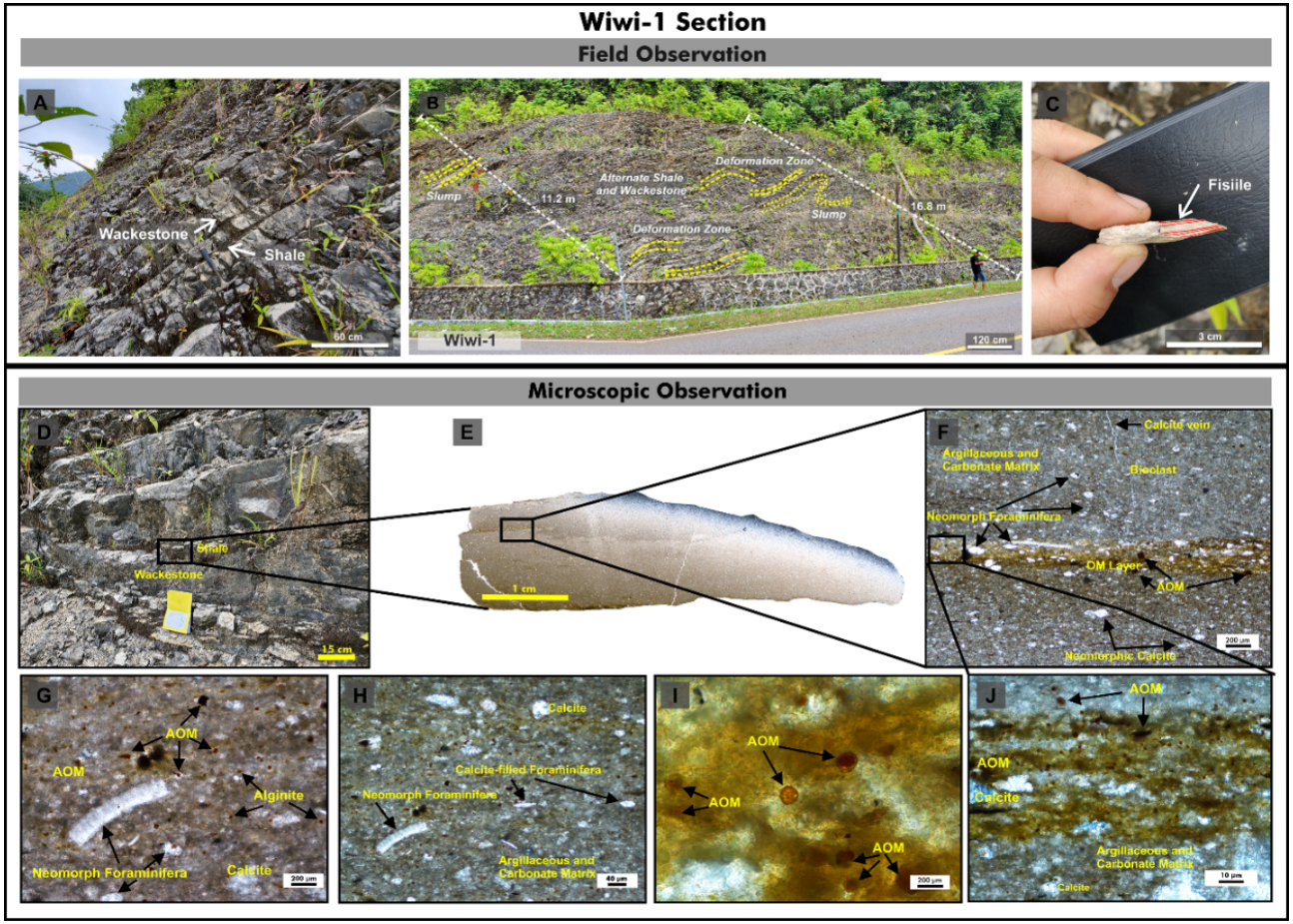

Figure 4. Field geological characteristics and microscopic observation of the Triassic-Jurassic Tokala Formation (based on geological map from Rusmana et al., 1993) cropped out in Wiwi-1 Section, Wiwirano Area, SE Sulawesi that indicated highly deformed strata (A). Tokala Formation cropped out in the Wiwirano area (Wiwi-1 section) with a thickness of approximately 22 meters composed of a thin shale layer (5- 12 cm) alternated with wackestone (A and D). The presence of meter-scale soft sedimentary structures, such as slumps, indicates the presence of a gravity-driven mass flow mechanism (B). Fissile structure was clearly observable during field observation (C). Organic matter concentrated as thin layer surrounded by argillceous and carbonate matrix, while dispersed organic matters including AOM depicted prominent in dispersed fashion (F). AOM occured incorporated with carbonate grain (e.g. calcite) and foraminifera that have undergone diagenesis forming neomorphic structures (G and H). High resolution AOM picture which scatterly distributed, surrounded by argillaceous and carbonate matrix (I and J).

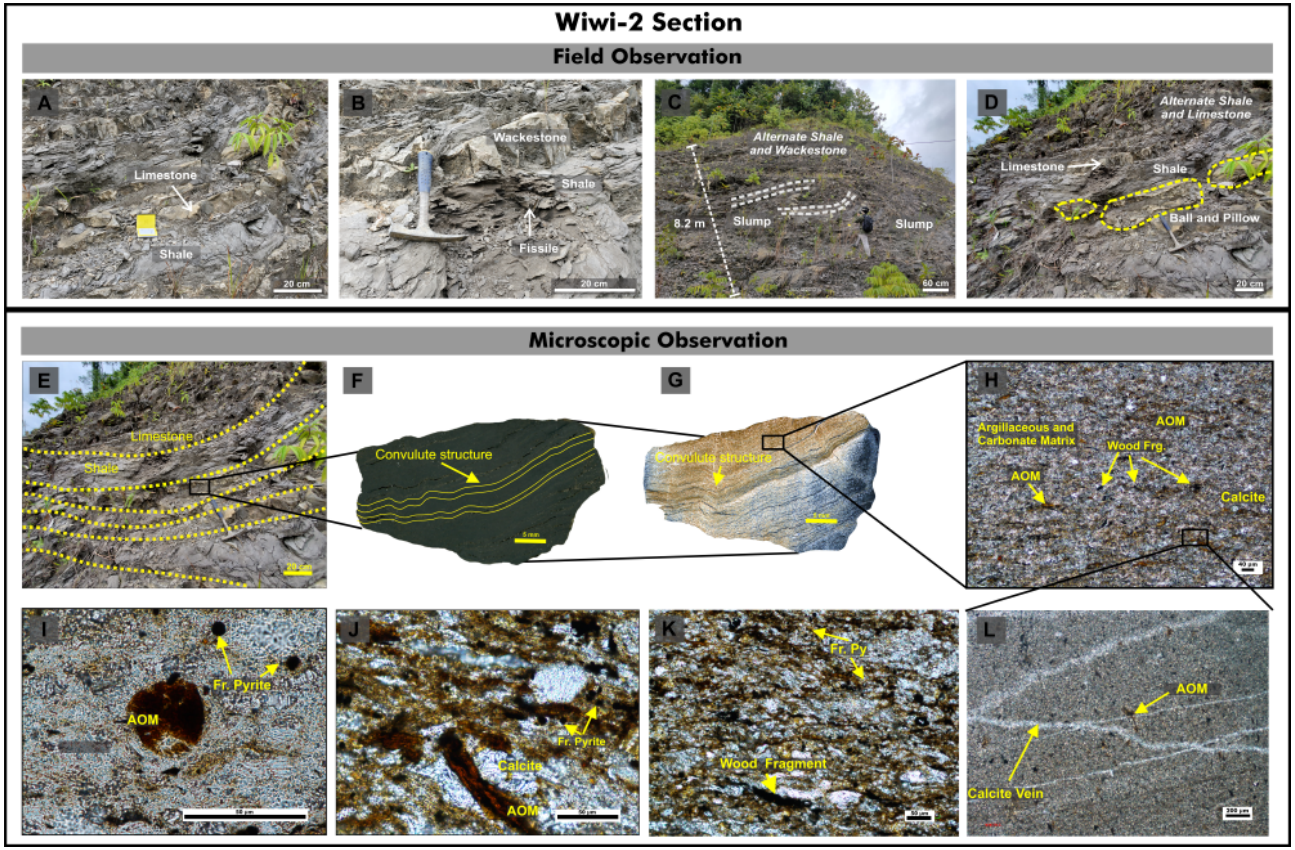

Figure 5. Field observation photos of Tokala Formation represented observed in Wiwi-2 section, Wiwirano Area, SE Sulawesi comprises alternated gray-shale with limestone which indicate high deformation intensity (A). Fissile structure in shale is clearly visible (B), while low angle sontourted contact between shale and limestone indicating gravity-mass flow (B and E), also corroborating with other sof sedimentary structures such as slump (C) and ball and pillow structure (D). Milimeter scale of sedimentary structure, such as convulute structure also depicted in polished rock chip surface (F and G). AOM incorporated with wood fragment in argillaceous and carbonate matrix, which show dispersed OM with ocassionally laminated (H-K). Pyrite framboidal (black cirle) was observed incoporated in various size from 6 – 17.5 µm (I-K). Skeletal grain occured intersected with calcite vein in Wiwi limestone sample (L).

Additionally, the lamination structure is prominently depicted on the polished surface of the rock chip, where micro-scale fractures within the rock matrix are observed filled with bitumen, indicative of hydrocarbon migration and accumulation processes (Figure 7 E and 7F). Under microscopic observation of the shale layer, vein calcite is observed intersecting the lamination, accompanied by streaks of bitumen (refer to Figure 7H and 7I). Organic matter accumulation is predominantly distributed in a laminated fashion, resulting in a distinctively organic matter lamination structure. This structure is further characterized by the incorporation of neomorph foraminifera and carbonate grains, as illustrated in Figure 7G, 7J, and 7K. However, based on these characteristics, the shale intervals also assigned as strongly laminated shale (SLS) facies, and interlayered limestone layer as foraminifera wackestone (FW) similar with those in Bule-1 section. One should be note, that all sections examined in this research are situated within newly exposed road cuts across the study area. These sections are consistently overlain by Quaternary deposits, indicating subsequent geological events and sedimentary processes that have significantly influenced the surface morphology in the region (Figure 1).

Matano Formation interval in the Prasasti-1 and Prasasti-2 sections have distinct characteristics compared to other sections, predominantly consisting of a 14.2-meter outcrop of massive mudstone and intercalation of limestone in the upper part (Figure 8A, 9B and 9C). At a quick glance, mudstone displays lighter color, massive, and looser compared to the previous section and fissility has not been formed (Figure 8K, 8C, and 9A).

Petrographically, a turbidite layer was noticed, which creates undulated contact with the underlying mudstone (Figure 8E). Turbidite layer composed of quartz, feldspar, mafic mineral, lithic fragment, and glauconite, with a size of coarse silt (0.03-0.04 mm), in argillaceous matrix (Figure 8E, and 8F). The texture of this turbidite layer is grain-supported, moderately sorted, subrounded–angular, and moderate sphericity. The underlain mudstone is dominantly composed of argillaceous material with lithic fragments, some quartz and mafic (pyroxene) clast together with AOM and woody OM (Figure 8D- 8F). Under microscopic observation, the argillaceous and carbonate matrices incorporated with scarce wood fragments and felsic minerals, including quartz and feldspar (refer to Figure 9D). Furthermore, the organic matter, in the form of amorphous organic matter (AOM), are dispersedly distributed and associated with the wood fragments and felsic quartz, suggesting a terrestrial input influence (as illustrated in Figure 9E). Based on these significant characteristics, these intervals are assigned as massive mudstone (MM).

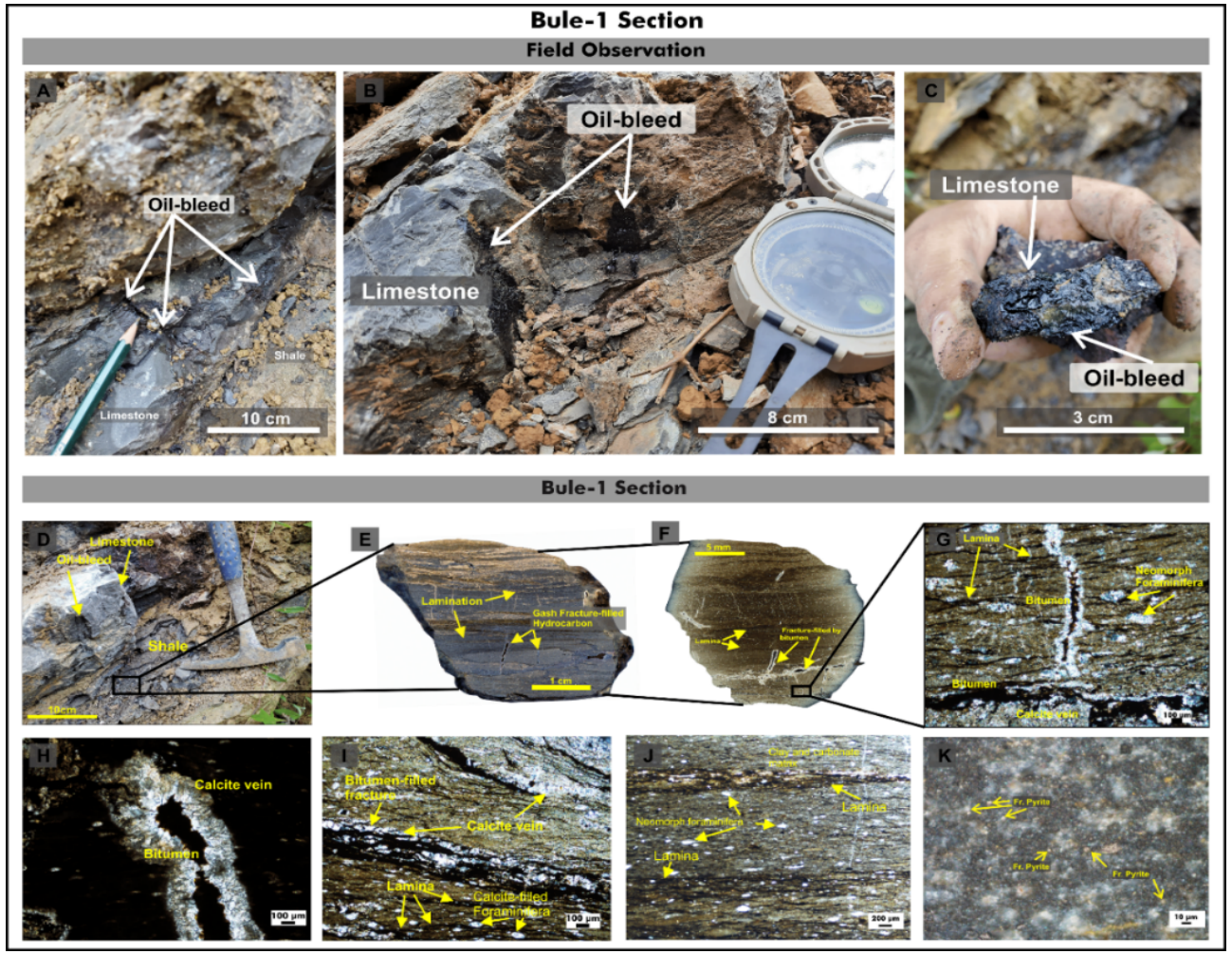

Figure 6. Highly deformed Tokala Formation outcrop founded in Buleleng area consist of alternating shale and limestone, notably the presence of oil-bleed within the fracture of limestone intervals (A-D). Lamination structure depicted in polished rock chip surface, together with micro-scale of fracture-filled bitumen (E and F). Thin section photography recorded OM in laminated form, intersected by fracture-filled by bitumen, while neomorphic structure is clearly visible (G and H). Note that neomoprh foraminifera occur in similar direction submerged in argillaceous and carbonate matrix indicating low energy during deposition (I – K).

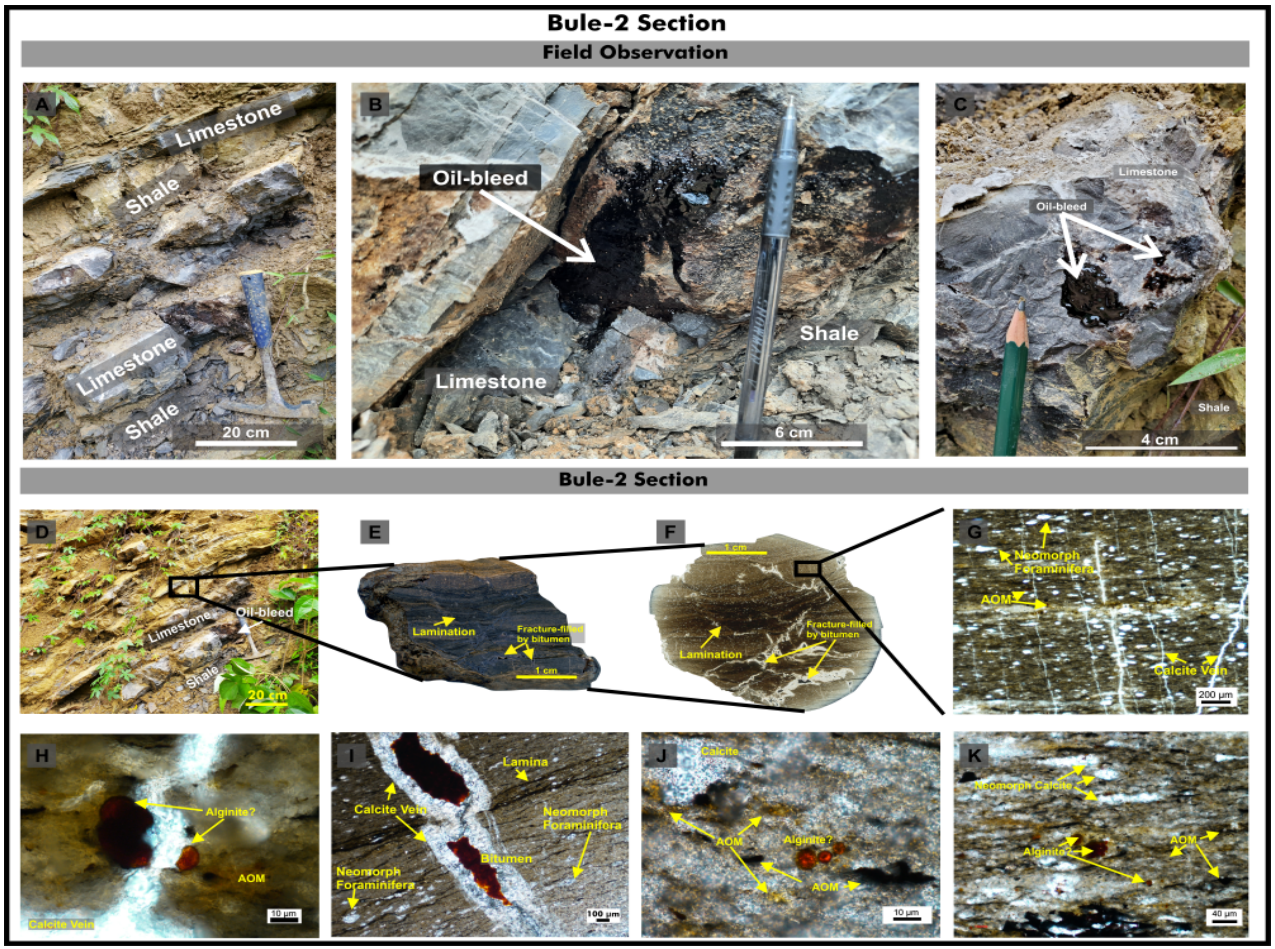

Figure 7. Alternating shale and limestone of Tokala Formation outcrop founded in Buleleng area, the presence of oil-bleed was observed occurred within the fracture of limestone intervals (A-D). Lamination structure depicted in polished rock chip surface, together with micro-scale of fracture-filled bitumen (E and F). Thin section photography recorded OM in laminated form, intersected by fracture-filled by bitumen, while neomorphic structure is clearly visible (G and H). Note that neomoprh foraminifera occur in similar direction submerged in argillaceous and carbonate matrix indicating low energy during deposition (I – K).

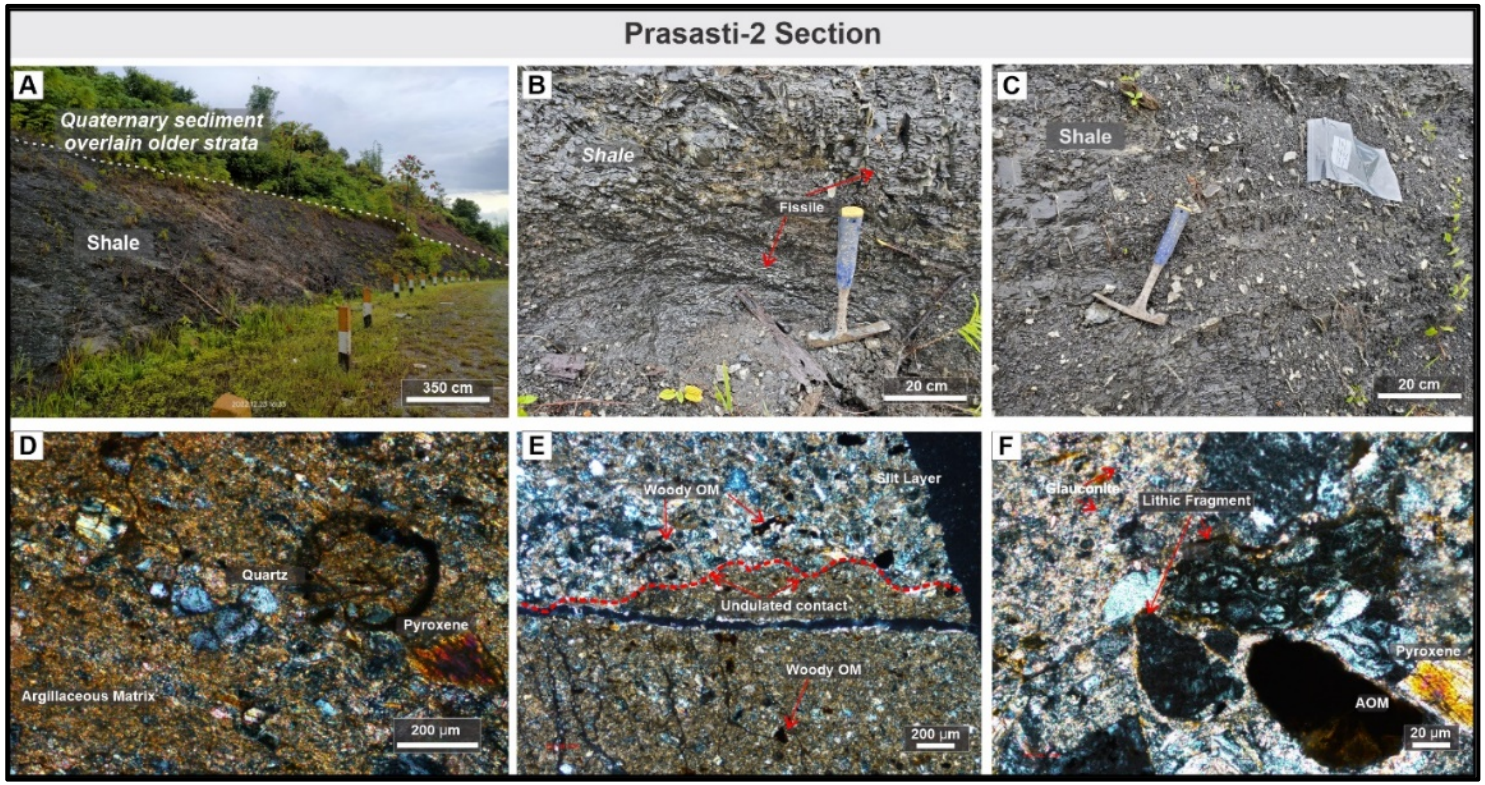

Figure 8. Field characteristics Matano Formation outcrop (based on geological map from Rusmana et al., 1993) in North Konawe to South Bungku road-cut. This outcrop consists of massive shale with approximate thickness 10.2 meters (A-C). Under microscopic observation, argillaceous and carbonate matrix are incoporated with scarce wood fragments, felsic minerals such as quartz, and feldspar (D). AOM incorporated with wood fragments and felsic quartz indicating terrestrial input influence (E).

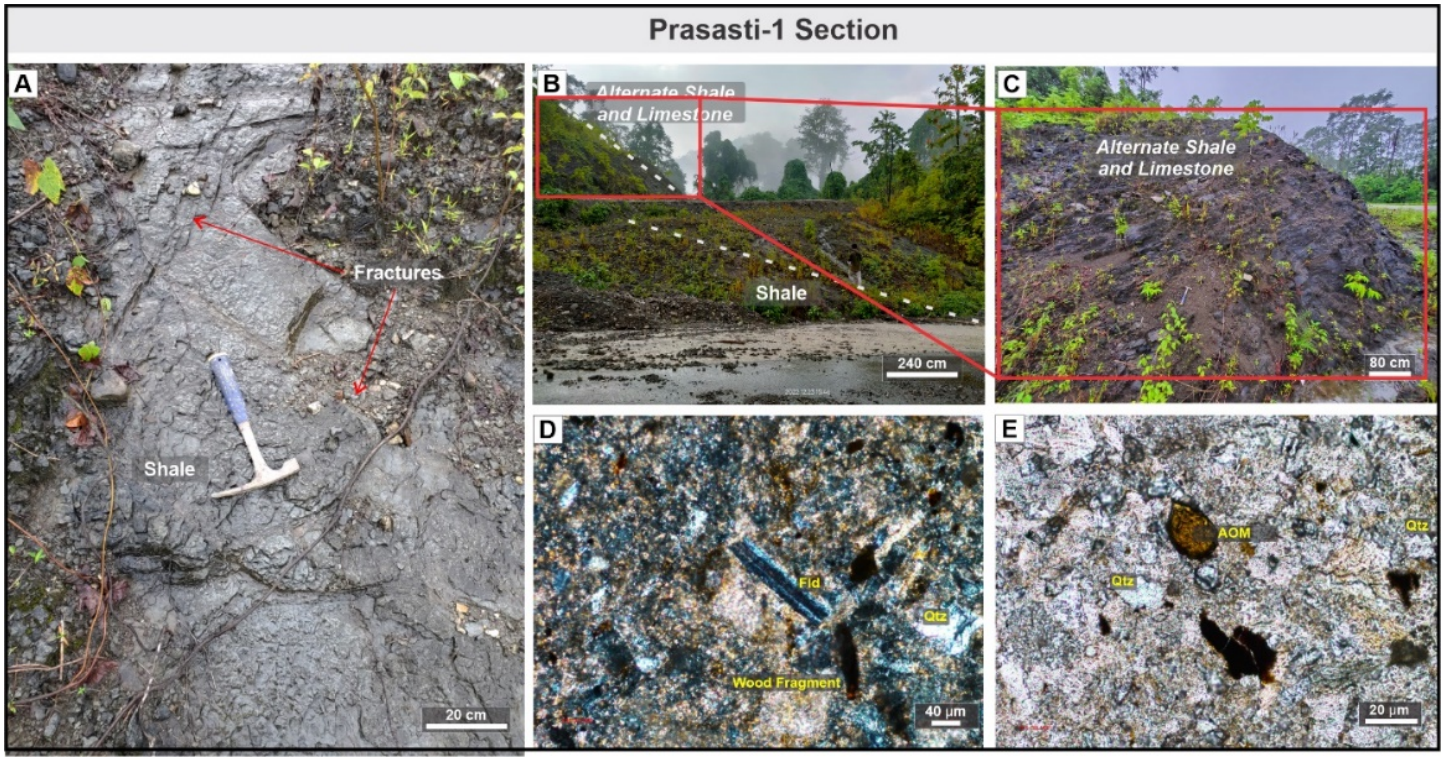

Figure 9. Field characteristics Matano Formation outcrop (based on geological map from Rusmana et al., 1993) in North Konawe to South Bungku road-cut. This outcrop consists of massive shale with approximate thickness 10.2 meters (A-C). Under microscopic observation, predominant argillaceous matrix are incoporated with scarce wood fragments, felsic minerals such as quartz, and feldspar (D). AOM incorporated with wood fragments and felsic quartz indicating terrestrial input influence (E).

4.2 Major and trace element composition

The major element geochemistry of shales revealed notable variances between the lithofacies. In general, SiO_2, Al_2O_3, and CaO are the dominant major oxides in our samples, where this composition is dependent on its lithology. Therefore, here we describe the major oxides composition restricted to these elements while the other oxides with relatively low composition are available in the Table 1. The Tokala shale in all sections (Wiwi-1, Wiwi-2, Bule-1, and Bule-2) characterized by predominant CaO (21.61-37.67%), accompanied by moderate SiO_2 (19.01-36.29%) and low Al_2O_3 (4.34-14.79%). Furthermore, the intercalated limestone was characterized by high CaO content (47.71-53.05%), low SiO_2 (3.45-8.74%), and extremely low Al_2O_3 (0.24-0.81%). Matano mudstone, on the other hand, demonstrated generally high SiO_2 content (42.53-46.07%), low Al_2O_3 (7.86-10.69%), and CaO (5.58-12.43%). Trace element composition of both shale and limestone of Tokala Formation and mudstone from the Matano Formation are presented in the Table 2. One should be noted that rubidium (Rb) and barium (Ba) display a negative correlation with strontium (Sr) in our samples. Furthermore, no significant LILEs differences between shale and limestone, except for Sr which is significantly concentrate in limestone. In addition, high-field strength elements (HFSEs; e.g., Zr and Nb) tend to scarce in the Tokala limestone, while these elements occurred in relatively moderate concentration in Tokala shale and Matano mudstone. Redox-sensitive trace elements (RSTEs; e.g., Cr, Ni, and V) are varied in all lithofacies as these elements are related to the redox condition during deposition.

4.3 TOC and pyrolysis results

The MM facies exhibit poor TOC (0.5-0.53%) and low hydrocarbon generation potential suggested by low S_2 (0.03-0.52 mgHC/g), potential yield (PY; 0.07-0.56 mgHC/g), and HI value (88-95), where the thermal maturity suggested by T_{max} value 426-434^{o}C. Different to MM facies, the Tokala shale tends to be richer in TOC and S_2 value and also higher HI (see Supplementary Data 1C). To be specific, Tokala shale from MS and WLS lithofacies sections demonstrated high TOC, respectively, 1.20-1.28% and 3.9-4.0%, where S_2 values were also correspondingly high at MS (2.05-2.06 mgHC/g) and WLS (17.04-18.46 mgHC/g), concurrent with excellent hydrogen index of 176-178 at MS and 448-466 in WLS. Similarly, shales from the SLS facies pointed to high TOC of 2.07-2.56%, S_2 values (7.28-12.13 mgHC/g) aligned with enriched hydrogen indices ranging from 384-472 Bule sections. In contrast, the thermal maturity within the Wiwi and Bule sections are considered as low, expressed in the T_{max} value range, respectively, 432-434^{o}C and 428-431^{o}C (detailed datasets available in Table 3).

Table 1. Major elements constituents from each facies with Rock-Eval Pyrolysis of Triassic-Jurassic shales of Tokala Formation and mudstone from Matano Formation

Section	Sample ID	Lithology	Lithofacies	Formation	SiO_2 (%)	TiO_2 (%)	Al_2O_3 (%)	Fe_2O_3 (%)	MnO (%)	MgO (%)	CaO (%)	K_2O (%)	P_2O_5 (%)
Wiwi-1	Wiwi-1A	Shale	Weakly-laminated shale	Tokala Fm.	24.07	0.59	10.55	3.82	0.02	1.41	28.69	1.28	0.10
	Wiwi-1B	Shale	Weakly-laminated shale	Tokala Fm.	24.06	0.60	10.54	3.81	0.02	1.41	28.67	1.30	0.10
	Wiwi-1C	Shale	Weakly-laminated shale	Tokala Fm.	23.16	0.52	11.33	3.78	0.02	1.43	28.72	1.25	0.10
	Wiwi1D	Shale	Weakly-laminated shale	Tokala Fm.	24.11	0.49	11.51	3.71	0.02	1.38	28.66	1.31	0.10
	Wiwi-1E	Shale	Weakly-laminated shale	Tokala Fm.	24.03	0.62	10.52	3.82	0.02	1.41	28.69	1.28	0.10
	Wiwi-1F	Shale	Weakly-laminated shale	Tokala Fm.	24.06	0.60	10.55	3.81	0.02	1.40	28.67	1.30	0.10
Wiwi-2	Wiwi-2A	Shale	Moderately-laminated shale	Tokala Fm.	35.60	0.63	14.51	3.37	0.03	1.69	17.91	1.40	0.04
	Wiwi-2B	Shale	Moderately-laminated shale	Tokala Fm.	36.29	0.63	14.75	3.52	0.03	1.94	17.87	1.40	0.05
	Wiwi-2C	Shale	Moderately-laminated shale	Tokala Fm.	35.60	0.63	14.51	3.37	0.03	1.69	17.61	1.40	0.04
	Wiwi-2D	Shale	Moderately-laminated shale	Tokala Fm.	36.29	0.63	14.15	3.53	0.03	1.93	17.88	1.40	0.05
	Wiwi-2E	Shale	Moderately-laminated shale	Tokala Fm.	36.60	0.61	14.31	3.47	0.03	1.93	17.93	1.41	0.04
	Wiwi-2F SH	Shale	Moderately-laminated shale	Tokala Fm.	35.49	0.56	14.35	3.42	0.03	1.91	17.87	1.42	0.05

	Wiwi-2G	Shale	Moderately-laminated shale	Tokala Fm.	35.56	0.64	13.96	3.49	0.03	1.87	18.34	1.42	0.04
	Wiwi-2H	Shale	Moderately-laminated shale	Tokala Fm.	36.19	0.61	14.55	3.53	0.03	1.97	17.95	1.41	0.05
	Wiwi-2I	Shale	Moderately-laminated shale	Tokala Fm.	35.48	0.65	14.58	3.57	0.03	1.83	17.94	1.41	0.04
	Wiwi-2J	Shale	Moderately-laminated shale	Tokala Fm.	35.39	0.62	14.65	3.33	0.03	1.72	17.88	1.43	0.05
	Wiwi-2A LS	Limestone	Wackestone	Tokala Fm.	8.74	0.09	2.31	0.81	0.04	0.31	47.71	0.12	0.02
	Wiwi-2B LS	Limestone	Wackestone	Tokala Fm.	8.72	0.08	2.33	0.79	0.04	0.29	47.73	0.15	0.02
Bule-1	Bule-1A	Shale	Strongly-laminated shale	Tokala Fm.	19.50	0.17	4.34	1.20	0.02	0.59	37.67	0.46	0.05
	Bule-1B	Shale	Strongly-laminated shale	Tokala Fm.	21.40	0.24	5.08	1.31	0.01	0.66	36.11	0.59	0.04
	Bule-1C	Shale	Strongly-laminated shale	Tokala Fm.	19.44	0.18	4.64	1.21	0.02	0.69	37.17	0.60	0.05
	Bule-1D	Shale	Strongly-laminated shale	Tokala Fm.	21.34	0.22	5.18	1.32	0.01	0.63	36.17	0.58	0.05
	Bule-1E	Shale	Strongly-laminated shale	Tokala Fm.	19.55	0.22	5.34	1.22	0.02	0.61	36.67	0.49	0.04
	Bule-1F	Shale	Strongly-laminated shale	Tokala Fm.	21.44	0.19	5.08	1.31	0.01	0.64	36.21	0.60	0.05
	Bule-1G	Shale	Strongly-laminated shale	Tokala Fm.	20.61	0.18	5.44	1.33	0.02	0.63	37.57	0.61	0.05
	Bule-1H	Shale	Strongly-laminated shale	Tokala Fm.	21.40	0.24	5.08	1.31	0.01	0.64	36.51	0.59	0.04
	Bule-1I	Shale	Strongly-laminated shale	Tokala Fm.	21.15	0.20	4.44	1.33	0.02	0.59	37.51	0.47	0.05
	Bule-1J	Shale	Strongly-laminated shale	Tokala Fm.	21.13	0.21	5.09	1.33	0.01	0.59	36.31	0.59	0.04

	Bule-1A LS	Limestone	Wackestone	Tokala Fm.	6.90	0.04	1.36	0.35	0.03	0.20	49.72	0.11	0.02
	Bule-1B LS	Limestone	Wackestone	Tokala Fm.	7.63	0.05	1.68	0.49	0.03	0.23	48.96	0.13	0.02
Bule-2	Bule-2A	Shale	Strongly-laminated shale	Tokala Fm.	23.46	0.27	7.27	1.63	0.02	0.74	32.38	0.64	0.05
	Bule-2B	Shale	Strongly-laminated shale	Tokala Fm.	19.50	0.18	4.34	1.20	0.02	0.59	37.67	0.48	0.05
	Bule-2C	Shale	Strongly-laminated shale	Tokala Fm.	23.66	0.28	6.62	1.53	0.02	0.72	32.68	0.61	0.05
	Bule-2D	Shale	Strongly-laminated shale	Tokala Fm.	19.55	0.18	5.54	1.22	0.02	0.55	37.67	0.61	0.05
	Bule-2E	Shale	Strongly-laminated shale	Tokala Fm.	21.80	0.18	7.17	1.63	0.02	0.56	32.58	0.64	0.04
	Bule-2F	Shale	Strongly-laminated shale	Tokala Fm.	20.50	0.20	5.34	1.22	0.02	0.59	37.68	0.63	0.05
	Bule-2G	Shale	Strongly-laminated shale	Tokala Fm.	22.46	0.20	7.27	1.43	0.02	0.54	33.48	0.64	0.05
	Bule-2H	Shale	Strongly-laminated shale	Tokala Fm.	22.50	0.21	5.64	1.53	0.02	0.59	33.77	0.48	0.04
	Bule-2I	Shale	Strongly-laminated shale	Tokala Fm.	23.01	0.23	7.07	1.63	0.02	0.74	32.78	0.64	0.05
	Bule-2J	Shale	Strongly-laminated shale	Tokala Fm.	19.50	0.23	4.44	1.32	0.02	0.73	37.57	0.64	0.05
	Bule-2A LS	Limestone	Wackestone	Tokala Fm.	3.59	0.04	0.82	0.27	0.02	0.23	53.02	0.02	0.03
	Bule-2B LS	Limestone	Wackestone	Tokala Fm.	3.45	0.03	0.76	0.24	0.02	0.22	53.05	0.02	0.03

Table 2. X-ray fluorescence (XRF) analysis data of quantitative trace element data for each defined lithofacies within the research area.

Section	Sample ID	Lithology	Lithofacies	Formation	Ba (ppm)	Cr (ppm)	Cu (ppm)	Nb (ppm)	Ni (ppm)	Pb (ppm)	Rb (ppm)	Sr (ppm)	V (ppm)	Y (ppm)	Zn (ppm)	Zr (ppm)
Wiwi-1	Wiwi-1A	Shale	Weakly-laminated shale	Tokala Fm.	20.10	71.4	6	3.9	34.4	8.5	51.6	975.7	165.9	10.9	65.1	51.7
	Wiwi-1B	Shale	Weakly-laminated shale	Tokala Fm.	20.13	71.2	6.5	3.88	34.4	8.52	51.61	975.3	166.3	10.8	65.2	51.6
	Wiwi-1C	Shale	Weakly-laminated shale	Tokala Fm.	20.11	71	6.1	4	37	8.4	52.7	972.1	160.9	10.5	60.1	56.7
	Wiwi1D	Shale	Weakly-laminated shale	Tokala Fm.	20.15	70.2	6.5	4	36.2	8.4	51.61	978.1	161.3	11.1	62.2	52.2
	Wiwi-1E	Shale	Weakly-laminated shale	Tokala Fm.	20.10	71.6	6.2	3.88	36	8.5	52	975.7	165.9	10.9	65.1	51.7
	Wiwi-1F	Shale	Weakly-laminated shale	Tokala Fm.	20.13	71.2	6.5	3.97	36	8.51	51.5	975.3	166.3	10.8	65.2	51.6
Wiwi-2	Wiwi-2A	Shale	Moderately-laminated shale	Tokala Fm.	53.00	72.2	23.6	17.2	54.5	11.6	62.9	597.8	293.8	14.1	72.7	79.4
	Wiwi-2B	Shale	Moderately-laminated shale	Tokala Fm.	50.90	74.8	26.8	10.9	54.5	11.3	62.2	677.9	324.8	16.0	54.5	80.4
	Wiwi-2C	Shale	Moderately-laminated shale	Tokala Fm.	53.00	75	23.2	17.2	55.5	11.6	62.9	597.8	293.8	14.0	72.7	79.4
	Wiwi-2D	Shale	Moderately-laminated shale	Tokala Fm.	50.89	74.6	26.4	10.88	55.2	11.32	62.19	677.8	324.7	16.1	54.4	80.5
	Wiwi-2E	Shale	Moderately-laminated shale	Tokala Fm.	53.00	72.2	23.6	11.2	53.3	11.8	63	697.8	293.8	14.1	72.7	79.4
	Wiwi-2F SH	Shale	Moderately-laminated shale	Tokala Fm.	51.90	74.7	25.2	17.3	45.4	11.5	63.8	677.9	324.8	16.0	54.5	80.4
	Wiwi-2G	Shale	Moderately-laminated shale	Tokala Fm.	53.00	74.8	26.2	11.2	53.3	11.8	63	592.1	293.8	14.0	72.7	79.4

	Wiwi-2H	Shale	Moderately-laminated shale	Tokala Fm.	52.89	74.6	26.4	17.3	45.4	11.5	63.8	662.8	324.7	16.1	54.4	80.5
	Wiwi-2I	Shale	Moderately-laminated shale	Tokala Fm.	53.22	73.4	24.4	11.2	53.3	11.8	63	567.8	293.8	14.0	72.7	79.4
	Wiwi-2J	Shale	Moderately-laminated shale	Tokala Fm.	52.89	73.3	26.6	17.3	45.4	11.5	63.8	687.8	324.7	16.1	54.4	80.5
	Wiwi-2A LS	Limestone	Wackestone	Tokala Fm.	44.00	79	4.7	1.5	54	5.5	17.4	1742.3	261.2	6.8	104.7	18.3
	Wiwi-2B LS	Limestone	Wackestone	Tokala Fm.	44.80	80	3.2	1.6	58.6	5	22.3	1684.6	280.3	8.6	102.6	20.3
Bule-1	Bule-1A	Shale	Strongly-laminated shale	Tokala Fm.	44.21	80.1	4.7	1.8	47.9	5.2	21.9	1742.3	261.2	6.8	104.7	18.3
	Bule-1B	Shale	Strongly-laminated shale	Tokala Fm.	44.78	80.2	4.7	2.7	65	4	24.3	1684.6	280.3	8.6	102.6	20.3
	Bule-1C	Shale	Strongly-laminated shale	Tokala Fm.	44.10	79.2	4.7	1.6	58.6	5	22.3	1742.3	261.2	6.8	104.7	18.3
	Bule-1D	Shale	Strongly-laminated shale	Tokala Fm.	44.81	78.5	4.2	1.8	47.9	5.2	21.9	1684.6	280.3	8.6	102.6	20.3
	Bule-1E	Shale	Strongly-laminated shale	Tokala Fm.	44.11	78.1	4.7	2.7	65	4	24.3	1742.3	261.2	6.8	104.7	18.3
	Bule-1F	Shale	Strongly-laminated shale	Tokala Fm.	44.11	78.1	4.1	2.9	54	5.4	24.5	1684.6	280.3	8.6	102.6	20.3
	Bule-1G	Shale	Strongly-laminated shale	Tokala Fm.	44.15	78.6	4.5	1.6	58.6	5	22.3	1742.3	261.2	6.8	104.7	18.3
	Bule-1H	Shale	Strongly-laminated shale	Tokala Fm.	44.80	80.4	4.2	1.5	53	5.5	17.4	1684.6	280.3	8.6	102.6	20.3
	Bule-1I	Shale	Strongly-laminated shale	Tokala Fm.	43.80	79.9	4.7	2.9	54	5.4	24.5	1377.6	289.6	5.7	65.5	29.0
	Bule-1J	Shale	Strongly-laminated shale	Tokala Fm.	44.00	98.6	5.7	1.5	50.4	5.5	17.4	1742.3	261.2	6.8	104.7	18.3
	Bule-1A LS	Limestone	Wackestone	Tokala Fm.	44.10	92.1	4.7	1.5	53	5.5	17.4	1377.6	289.6	5.7	65.5	29.0

	Bule-1B LS	Limestone	Wackestone	Tokala Fm.	44.12	95.1	5.1	1.6	53.7	4.4	17.3	1742.3	261.2	6.8	104.7	18.3
Bule-2	Bule-2A	Shale	Strongly-laminated shale	Tokala Fm.	43.80	90.1	5.6	1.8	47.9	5.2	21.9	1377.6	289.6	5.7	65.5	29.0
	Bule-2B	Shale	Strongly-laminated shale	Tokala Fm.	43.77	89.2	3.2	2.7	65	4	24.3	1742.3	261.2	6.8	104.7	18.3
	Bule-2C	Shale	Strongly-laminated shale	Tokala Fm.	43.77	92.1	5.7	1.5	50.4	5.5	17.4	1377.6	289.6	5.7	65.5	29.0
	Bule-2D	Shale	Strongly-laminated shale	Tokala Fm.	44.00	90.1	4.7	1.5	53	5.5	17.4	1742.3	261.2	6.8	104.7	18.3
	Bule-2E	Shale	Strongly-laminated shale	Tokala Fm.	43.78	89.2	5.1	1.6	53.7	4.4	17.3	1377.6	289.6	5.7	65.5	29.0
	Bule-2F	Shale	Strongly-laminated shale	Tokala Fm.	44.11	95.2	3.3	2.7	65	4	24.3	1742.3	261.2	6.8	104.7	18.3
	Bule-2G	Shale	Strongly-laminated shale	Tokala Fm.	33.10	0	0	0.8	2	2.5	4.2	2076.4	85.7	0.0	8.7	0.9
	Bule-2H	Shale	Strongly-laminated shale	Tokala Fm.	36.80	0	0	1.1	2.2	2.3	5.4	1990.9	92.6	0.0	13.3	2.5
	Bule-2I	Shale	Strongly-laminated shale	Tokala Fm.	34.00	0	0	0.5	0	1.6	1.4	1473.0	17.3	0.6	4.8	3.0
	Bule-2J	Shale	Strongly-laminated shale	Tokala Fm.	22.90	0	0	0.6	0	1.7	1.4	1516.4	10.7	0.6	3.1	2.3
	Bule-2A LS	Limestone	Wackestone	Tokala Fm.	33.77	0	0	0.2	0	2.5	7.88	1402.0	38.7	7.3	4.9	19.0
	Bule-2B LS	Limestone	Wackestone	Tokala Fm.	33.80	0	0	0.2	0	2.5	7.9	1402.5	38.8	7.5	4.6	19.3

Table 3. TOC and Rock-Eval Pyrolysis data of all the samples from each sections including formation, lithology, and facies observed in this research.

Section	Sample ID	Lithology	Lithofacies	Formation	S1 (mg/g)	S2 (mg/g)	S3 (mg/g)	S1+S2 (PY)	TOC (wt.%)	HI (mgHC/gTOC)	OI (mgHC/gTOC)	Tmax (ºC)
Wiwi-1	Wiwi-1A	Shale	Weakly-laminated shale	Tokala Fm.	0.07	2.06	2.06	2.13	1.17	176	62	437
	Wiwi-1B	Shale	Weakly-laminated shale	Tokala Fm.	0.08	2.05	2.05	2.13	1.16	178	60	437
	Wiwi-1C	Shale	Weakly-laminated shale	Tokala Fm.	0.08	2.16	2.16	2.24	1.19	182	55	436
	Wiwi1D	Shale	Weakly-laminated shale	Tokala Fm.	0.07	2.03	2.03	2.10	1.15	177	56	437
	Wiwi-1E	Shale	Weakly-laminated shale	Tokala Fm.	0.07	2.03	2.03	2.10	1.14	178	54	437
	Wiwi-1F	Shale	Weakly-laminated shale	Tokala Fm.	0.07	2.06	2.06	2.13	1.17	176	62	437
Wiwi-2	Wiwi-2A	Shale	Moderately-laminated shale	Tokala Fm.	0.77	17.42	17.42	18.19	3.90	448	8	435
	Wiwi-2B	Shale	Moderately-laminated shale	Tokala Fm.	0.60	18.45	18.45	19.05	3.96	466	9	435
	Wiwi-2C	Shale	Moderately-laminated shale	Tokala Fm.	0.70	17.42	17.42	18.12	3.90	447	7	436
	Wiwi-2D	Shale	Moderately-laminated shale	Tokala Fm.	0.75	18.46	18.46	19.21	4.05	464	11	435
	Wiwi-2E	Shale	Moderately-laminated shale	Tokala Fm.	0.75	18.51	18.51	19.26	3.94	470	8	435
	Wiwi-2F SH	Shale	Moderately-laminated shale	Tokala Fm.	0.74	18.2	18.2	18.94	3.95	461	8	435

	Wiwi-2G	Shale	Moderately-laminated shale	Tokala Fm.	0.67	20.24	20.24	20.91	4.05	500	9	434
	Wiwi-2H	Shale	Moderately-laminated shale	Tokala Fm.	0.51	15.63	15.63	16.14	3.33	469	9	435
	Wiwi-2I	Shale	Moderately-laminated shale	Tokala Fm.	0.77	17.42	17.42	18.19	3.9	447	7	434
	Wiwi-2J	Shale	Moderately-laminated shale	Tokala Fm.	0.60	18.45	18.45	19.05	3.96	466	9	433
	Wiwi-2A LS	Limestone	Wackestone	Tokala Fm.	0.01	0.76	0.76	0.77	0.33	230	88	440
	Wiwi-2B LS	Limestone	Wackestone	Tokala Fm.	0.05	0.75	0.75	0.80	0.29	229	81	439
Bule-1	Bule-1A	Shale	Strongly-laminated shale	Tokala Fm.	0.07	12.13	12.13	12.20	2.57	472	26	437
	Bule-1B	Shale	Strongly-laminated shale	Tokala Fm.	0.06	7.34	7.34	7.40	2.07	394	35	437
	Bule-1C	Shale	Strongly-laminated shale	Tokala Fm.	0.07	12.1	12.1	12.20	18.3	497	24	432
	Bule-1D	Shale	Strongly-laminated shale	Tokala Fm.	0.07	7.3	7.3	7.41	20.3	479	25	434
	Bule-1E	Shale	Strongly-laminated shale	Tokala Fm.	0.07	13.1	13.1	13.20	18.3	483	25	434
	Bule-1F	Shale	Strongly-laminated shale	Tokala Fm.	0.07	12.2	12.2	12.23	20.3	489	33	434
	Bule-1G	Shale	Strongly-laminated shale	Tokala Fm.	0.07	12.8	12.8	12.87	18.3	472	26	434
	Bule-1H	Shale	Strongly-laminated shale	Tokala Fm.	0.06	12.9	12.9	12.93	20.3	355	35	434
	Bule-1I	Shale	Strongly-laminated shale	Tokala Fm.	0.07	12.1	12.1	12.20	18.3	497	24	434

	Bule-1J	Shale	Strongly-laminated shale	Tokala Fm.	0.07	7.3	7.3	7.41	20.3	479	25	432
	Bule-1A LS	Limestone	Wackestone	Tokala Fm.	0.09	2.41	2.41	2.50	0.56	430	54	427
	Bule-1B LS	Limestone	Wackestone	Tokala Fm.	0.09	3.55	3.55	3.64	0.79	449	41	424
Bule-2	Bule-2A	Shale	Strongly-laminated shale	Tokala Fm.	0.11	13.13	13.13	13.24	2.07	423	39	435
	Bule-2B	Shale	Strongly-laminated shale	Tokala Fm.	0.04	12.16	12.16	12.20	2.52	472	26	436
	Bule-2C	Shale	Strongly-laminated shale	Tokala Fm.	0.04	7.28	7.28	7.32	2.07	343	36	434
	Bule-2D	Shale	Strongly-laminated shale	Tokala Fm.	0.03	12.13	12.13	12.16	2.52	350	33	434
	Bule-2E	Shale	Strongly-laminated shale	Tokala Fm.	0.04	7.28	7.28	7.32	2.07	344	34	434
	Bule-2F	Shale	Strongly-laminated shale	Tokala Fm.	0.04	12.13	12.13	12.17	2.52	423	35	435
	Bule-2G	Shale	Strongly-laminated shale	Tokala Fm.	0.11	7.28	7.28	7.39	2.07	339	39	435
	Bule-2H	Shale	Strongly-laminated shale	Tokala Fm.	0.04	12.13	12.13	12.17	2.52	349	33	434
	Bule-2I	Shale	Strongly-laminated shale	Tokala Fm.	0.04	7.28	7.28	7.32	2.07	343	36	432
	Bule-2J	Shale	Strongly-laminated shale	Tokala Fm.	0.03	12.13	12.13	12.16	2.52	346	33	435
	Bule-2A LS	Limestone	Wackestone	Tokala Fm.	0.14	0.09	0.09	0.23	0.07	90	210	452
	Bule-2B LS	Limestone	Wackestone	Tokala Fm.	0.01	0.09	0.09	0.10	0.10	129	371	448

4.4 Biomarker characteristics

Selected outcrop samples underwent further biomarker analysis to perform refined geochemical characterization. Specifically, two samples were evaluated from WLS facies and each representative sample from SLS Bule-1, SLS Bule-2, and Bule oil stain. Pristane and phytane biomarkers were also quantified, revealing pr/ph ratios of 2.30, 0.98, and 1.27 for the Tokala shale, respectively, in the WLS, SLS Bule-1, and SLS Bule-2 facies, together with a ratio of 0.78 for the Bule oil stain. The conducted biomarker analysis revealed distinct paleoenvironmental signatures between all shale samples. Specifically, C_{29} diahopanes and 28-30-bisnorhopanes peaks, were conspicuously present in the Tokala shale from Wiwi-2 samples but absent in the SLS Bule-1, SLS Bule-2 facies, and oil stain. Meanwhile, the C_{35}/C_{34} homohopanes ratio, displayed only moderate values amongst the Bule units. As carbonate-influenced content was significantly concentrated, parameters indicative of such settings, including the 30-norhopanes series, Tm/Ts ratio, C_{29}/C_{30} hopanes, and diasteranes/steranes ratio, were carefully evaluated. Results point to all SLS samples and oil exhibiting 30-norhopanes series, high Tm/Ts ratios, and C_{29}/C_{30} hopanes. Concurrently, in the Wiwi-2 samples, attributed with relatively low Tm/Ts and C_{29}/C_{30} hopanes but enriched diasteranes/steranes (Table 4; Supplementary Data 2A).

Table 3. Biomarker parameters data for paleoenvironment determination within this research, obtained from rock extract from each lithofacies (e.g. weakly laminated shale/WLS and strongly laminated shale /SLS)

No	Lithofacies	Pr/Ph	Tm/Ts	C_{35}/C_{34} Homohopanes	C_{29}/C_{30} Hopanes	Diastreanes/Steranes
1	Weakly laminated shale (WLS)	2.39019	0.52	0.82	0.39	1.09
2	Weakly laminated shale (WLS)	2.39019	0.47	0.85	0.39	1.12
3	Strongly laminated shale (SLS)	0.98	6.74	0.73	2.34	0.53
4	Strongly laminated shale (SLS)	1.56	6.77	0.72	2.29	0.52

Chapter V: DISCUSSION

5.1 Lithofacies correlation with regional stratigraphy

All stratigraphic intervals in this study are dominantly composed of the interbedding of limestone and shale with various thickness proportions. Since the age data and was not available in this study, the formation was assigned based on the regional lithostratigraphy (Surono and Hartono, 2013). This observation leaves three carbonate formations within the research area that could be correlated with our carbonate intervals, such as Triassic-Jurassic Tokala, Cretaceous Matano, and Paleogene Tampakura Formations (Rusmana et al., 1993; Surono and Bachri, 2002; Surono and Hartono, 2013; Nugraha and Hall, 2022). Carbonate intervals traversed in all sections tend to be correlated with the Triassic-Jurassic Tokala Formation for several reasons. First, the Tokala Formation is composed of marl, bioclastic limestone, argillaceous limestone, micritic limestone, and black shale related to the carbonate platform environment (Simandjuntak et al., 1993; Surono and Hartono, 2013), which share similar characteristics with our marine carbonates. Bioclastic and micritic limestones (Surono and Hartono, 2013), respectively, are represented by FW and LM facies, while black shale facies (Surono and Hartono, 2013) is comprised of MS, WLS, and SLS facies. Surono and Bachri (2002) also pointed out that turbidite deposits occurred intercalating with limestone in the Tokala Formation. This point is in line with our findings about gravity mass flow deposit (GMF) in the formation evidenced by the occurrence of soft sedimentary structures (Boggs Jr., 2005; Nichols, 2009).

Additionally, Surono and Hartono (2013) found belemnite fossils only in the Tokala Formation, where we also noticed this fossil in the Bule section. Second, the Tokala Formation was deposited during the Gondwana break-up (Santy, 2016; Surono and Hartono, 2013), consequently, sediments were supplied from continental granitic source that was rich in quartz (Rudyawan and Hall, 2012; Nugraha and Hall, 2022), while mafic and lithic volcanic constituents indicate post-break-up sedimentation (Dickinson, 1985; Taylor and Mclennan, 1995). In all sections, these constituents were absent, while quartz might exist in a low concentration, supporting that our carbonates are part of syn-rift basin fill. Last, our carbonate has undergone extreme diagenesis, specifically neomorphism, that indicates deep burial (Ulmer-Scholle et al., 2014), which might only be achieved in the older strata.

The MM interval in the Prasasti-1 and Prasasti-2 sections is interpreted to be part of the Matano Formation (Rusmana et al., 1993) that has different genetics from other shale outcrops. First, mafic and lithic constituents were found within the mudstone interval, suggesting that, at least, sediments were deposited after the break-up event (post-Cretaceous; Surono and Hartono, 2013; Nugraha and Hall, 2022). Second, our mudstone tends to be loose regarding crystallinity,

indicating a relatively younger age than other sections. This mudstone was subjected as a drift unit (post-break-up) and potentially correlated with the Cretaceous Matano Formation (Rusmana et al., 1993; Surono and Hartono, 2013). Therefore, our outcrop-to-microscale lithological description is indeed linked with regional stratigraphy and could be used for further interpretation.

5.2 Petrochemistry of Pre-Tertiary shales in the Southeast of Sulawesi

As lithofacies mean that the body of rock should be distinguishable from each other based on its lithological characteristics, the scope and scale of facies determination became crucial. The scale-matter is complicated, especially in mudstone, for example “well-bedded mudstone” observed in the field, could be a “massive mudstone” under the thin section. To simplify the complexities, for further geochemical interpretation, Three major constituents are commonly used for mudstone and shale classification, which are quartz, carbonates, and clay minerals (Ulmer-Scholle et al., 2014; Rojas et al., 2016; Mews et al., 2019), which are usually obtained from XRD analysis. Whilst quantitative mineralogical data is not available, this study classified Tokala shale based on major element contents retrieved from XRF analysis (Table 1). Element-based classification itself is not new, for example, Herron (1988) proposed chemical discrimination for sedimentary rocks, where specifically shales were divided into "shale" and "Fe-shale", while the percentage of Al2O3 was further interpreted to be related to grain size (Sprague et al., 2009). However, in our case, it is totally confirmed that all of the samples could be considered mudstone (sensu stricto) or even shale as fissility was observed. Therefore, we proposed a direct elemental-based classification that is related to three major shale components (Ulmer-Scholle et al., 2014; Rojas et al., 2016; Mews et al., 2019), in which quartz, carbonate, and clay minerals are respectively represented by SiO2, CaO, and Al2O3. The elemental representation of these minerals was justified with the correlation between each element (Figure 10), for example, a negative correlation between CaO with SiO2 and Al2O3 means that increasing carbonate proportion will reduce argillaceous and siliceous minerals (and CaO is not related to other Ca-bearing minerals like chlorite). Hence, this scheme distinguished three groups, such as argillaceous, "mixed", and calcareous shales (Figure 11).

As a consequence of elemental-based classification, the term "mixed" could occur in various forms, such as lamination between carbonate and clay mineral grains, clay mineral as structural grains, clay mineral as cement and matrix, or a combination of these three scenarios (Figure 11; Schlumberger, 2005). The "mixed" group of Tokala Formation is characterized by relatively moderate concentrations of SiO_2, Al_2O_3, and CaO. Petrographic analysis confirms that this group occurred at least as a combination of lamination and dispersed shales. Tokala shale from Wiwi and Bule sections were classified into this group (later referred to Wiwi and

Bule ”mixed” shale). Therefore, the elemental composition of shales successfully classified the complexities of Tokala and Matano lithofacies into several groups for further geochemical interpretation. It seems elemental classification could be related to paleo-depositional conditions that control organic matter enrichment, instead using complex lithofacies discrimination, chemofacies were applied for further discussion.

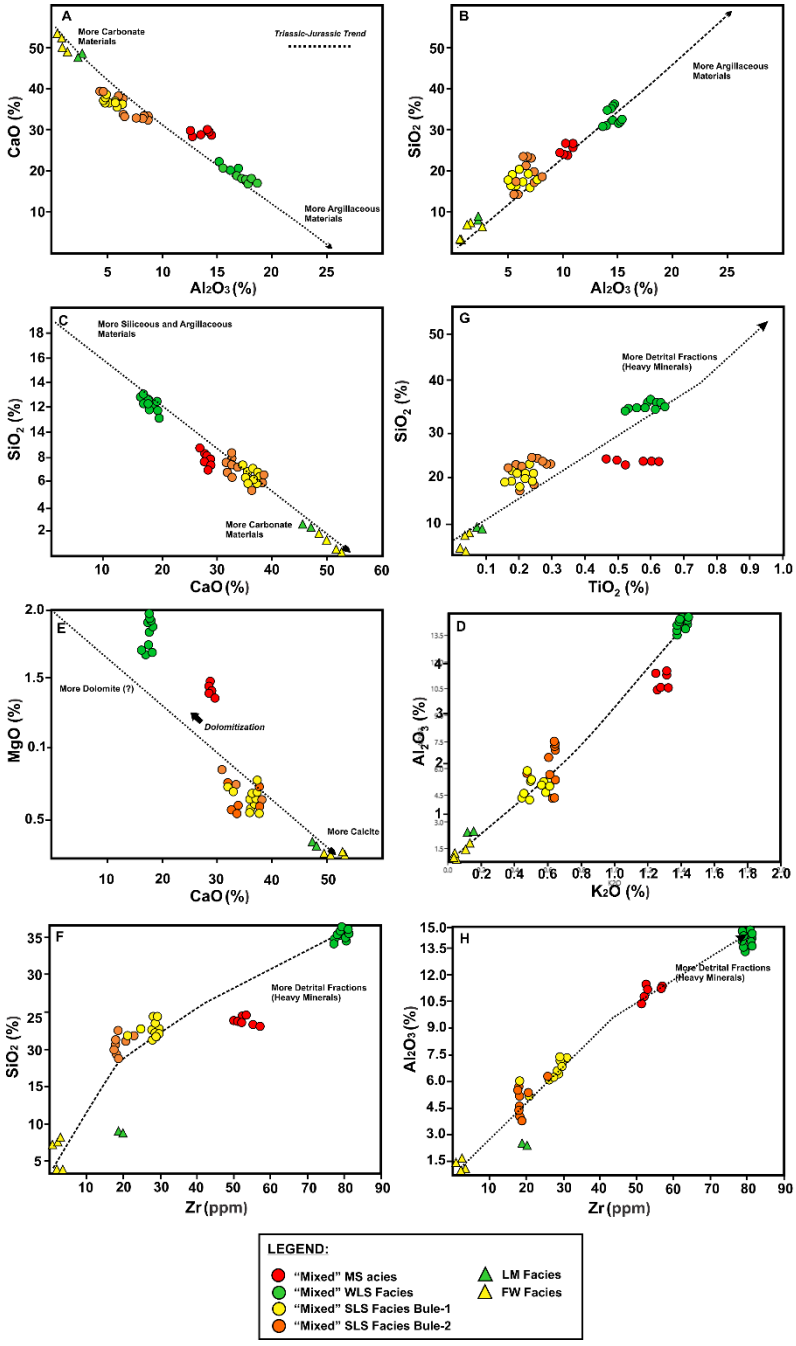

Figure 10. Several correlation plots were generated to obtain the relationship between each element, facilitating predictions regarding shale mineralogical content. For example, SiO2 is increased together with Al2O3 which might be related to clay minerals (alumino-silicates). Moreover, CaO and Al2O3 show a negative correlation, in which Ca is interpreted to be not related to Ca-rich clay minerals (e.g. chlorite) but rather to carbonate minerals (e.g. calcite). See text for full explanations

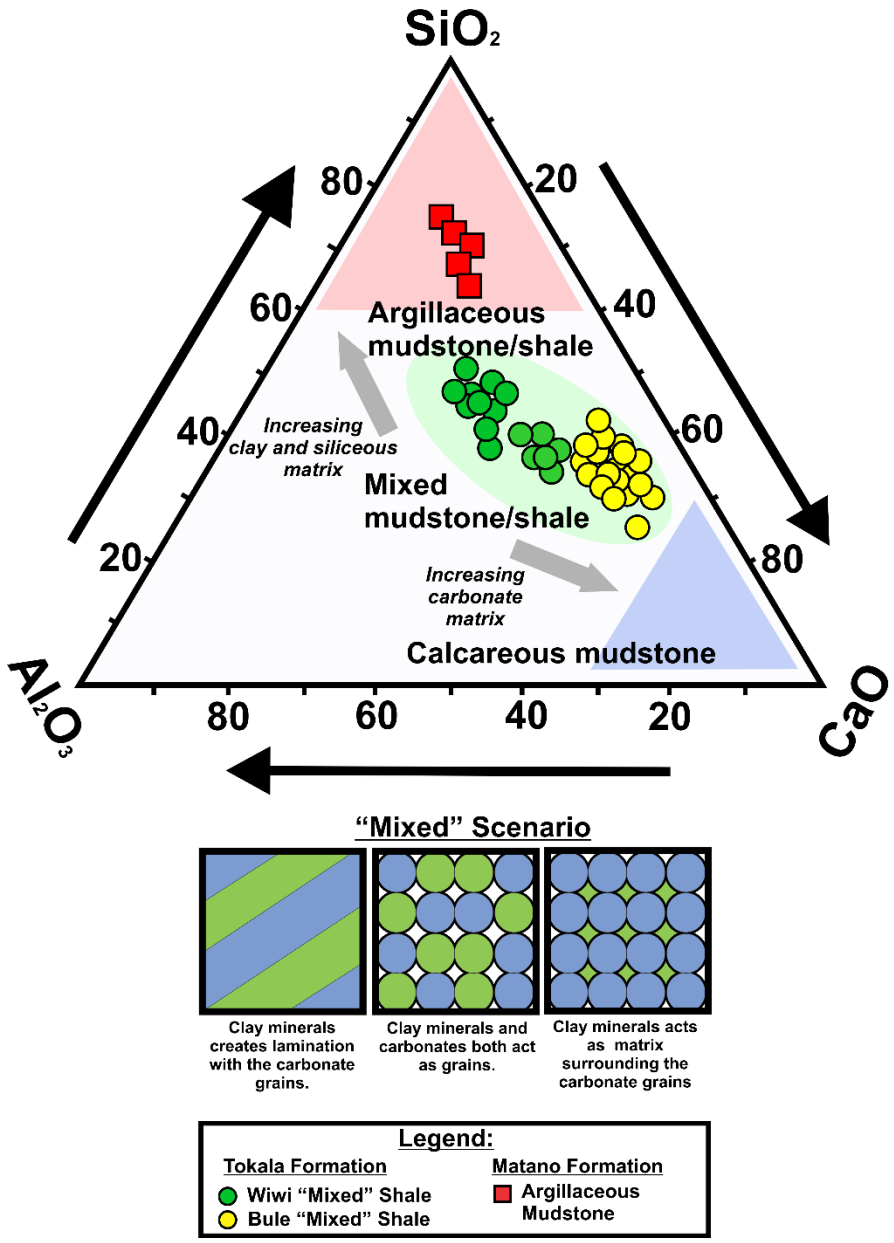

Figure 11. Proposed shale and mudstone classification based on elemental content, which reflects major shale mineralogical constituents, quartz, carbonates, and clay minerals (Ulmer-Scholle et al., 2014; Rojas et al., 2016; Mews et al., 2019). Correlations between each element are observed to link the major elements and shale mineralogy, in which our samples were divided into argillaceous, and "mixed" shales. As the classification is based on elemental composition, the term "mixed" could occur in various forms, such as lamination, grains, cement and matrix, or a combination of these three scenarios (Hurst, 1986; Molenaar, 2021).

5.3 Source rock characteristics: maturity, quantity, and quality

In order to discuss carbonate source rock characteristics, further organic enrichment mechanism of each facies, and depositional environment, thermal maturity information is compulsory to understand. The reason is that source rock maturation process could significantly reduce TOC and S2 values (Jarvie et al., 2007; Dembicki Jr., 2017; Huo et al.,

2019) which these affected values will not represent the initial organic matter conditions. From our dataset, all facies could be considered as early mature (Tmax 434-435°C; Peters and Cassa, 1994) so that source rock characterization could be done further.

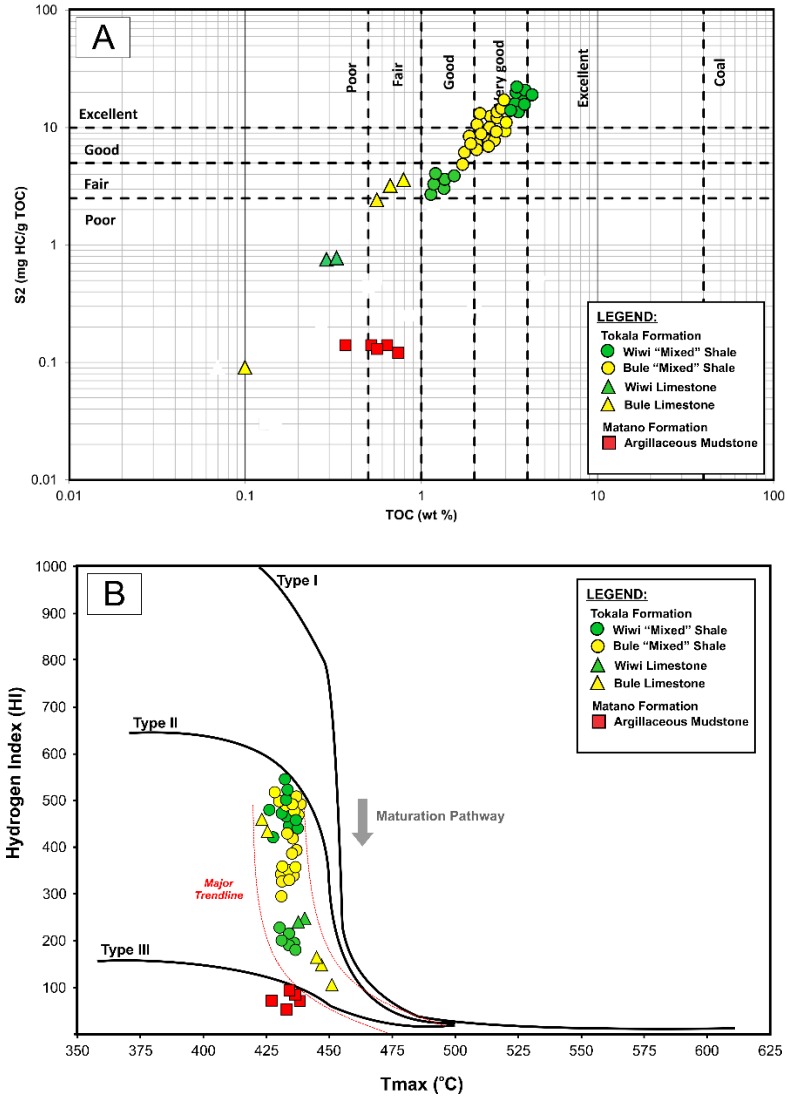

Figure 12. The quantity of organic matter represented by total organic carbon (TOC) and S2 values and quality of organic matter inferred from the pseudo-van Krevelen diagram (classification from Peters and Cassa, 1994; Dembicki Jr., 2009). Argillaceous shale from the Tokala Formation exhibits poor TOC and HI while these facies are composed dominantly of type III and type IV kerogen, respectively. Concurrently, Tokala "mixed" shale exhibits excellent organic matter quantity expressed by high TOC and excellent HI value. While the Tokala "mixed" shale and limestone fall outside the type II regression line, these samples give a similar type II kerogen trendline.

Argillaceous mudstone facies suggested low hydrocarbon generation potential (S_2 and PY) aligned with low HI value indicating that this facies are dominantly composed of type III kerogen (Peters and Cassa, 1994). In comparison, the argillaceous Tokala shale also comprises low TOC and depleted in hydrogen-rich organic matter which is probably composed of type IV kerogen indicated by extremely low HI. Concurrently, the "mixed" Tokala facies (Wiwi

and Bule “mixed” shales), have excellent hydrocarbon source rock characteristics which are expressed by excellent TOC and S_2 values followed by elevated HI indicating type II kerogen contribution (Figure 12A and 12B). Both qualitative organic matter assessments from visual observation (petrographic analysis) and indirect measurement (pyrolysis analysis) were matched. With an example from the argillaceous mudstone, samples with low HI have a relatively significant amount of wood fragment (Figure 5L and 5M). Another good example was recorded in all “mixed” shale facies of Tokala Formation where high HI is correlated with the abundance of fluorescence AOM, which are sedimentation rate and redox condition (Demaison and Moore, 1980; Dembicki Jr, 2017). It is clearly recorded from both petrography and inorganic geochemistry analysis that argillaceous materials are probably rapidly deposited and potentially dilute the OM (Tissot and Welte, 1987; Bordenave, 1993; Dembicki Jr, 2017).

This study also linked to the relation between the carbonate-siliciclastic ratio that represents sedimentation processes, and source rock quantity and quality. We observed that the increasing carbonate content, represented by CaO, is followed by a slight decrease in TOC and hydrocarbon generative potential (Figure 13). Moreover, high input of siliciclastic material, represented by SiO_2, is also followed by decreasing source rock quantity and quality. Therefore, it is believed that the quantity and quality of organic matter, specifically in carbonate source rock, are an equilibrium of carbonate and siliciclastic content related to sedimentation processes. Slow carbonate accumulation exhibits poor organic matter preservation, resulting in the degradation of organic matter. Concurrently, rapid siliciclastic transportation and sedimentation during mudstone deposition potentially dilute the OM concentration with high clay input (Tissot and Welte, 1984; Dembicki Jr., 2017). However, one intriguing aspect that we should also consider related to the lack OM preservation is potential influence of bioturbation activity on the preservation quality of organic matter, particularly concerning its impact on total organic carbon (TOC) content within carbonate rocks (Jones, 1984). However, contrary to expectations, our investigation reveals that despite bioturbation affecting the Wiwi “mixed” shales, the TOC values remain robust. This condition could potentially be attributed to the significant presence of argillaceous material, characterized by high clay content, which has a propensity to adsorb organic matter (Cordell, 1992), which indicated by positive correlation between Al_2O_3 and TOC in Wiwi “mixed” shales (Figure 13). This complex interplay of factors underscores the mechanisms governing organic matter preservation within carbonate lithofacies in relation to the organofacies variation.

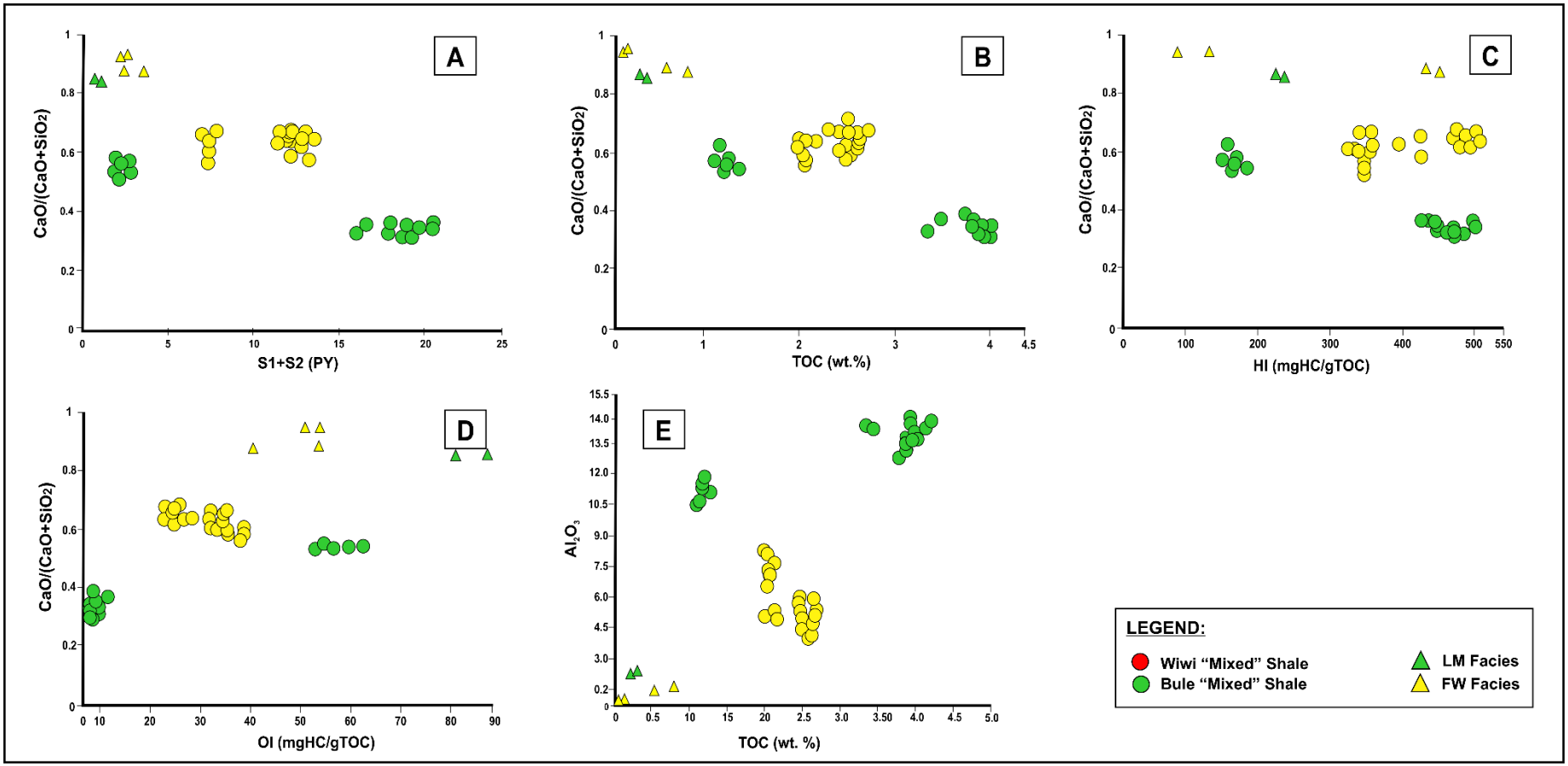

Figure 13. Bivariate plots of CaO/(CaO+SiO2), which represents the carbonate-siliciclastic ratio and could be taken further for sedimentation processes, versus PY (A), TOC (B), HI (C), OI (D), and S2/S3. The graphs show negative correlations between CaO/SiO2 with the quantity of organic matter, in which increasing carbonate content is followed by a slight decrease in TOC and hydrocarbon generative potential, and vice versa. The positive correlation also indicated by Al_2O_3 vs TOC which related to the clay concentration in relation with OM preservation. See text for full explanation.

5.4 Organofacies and paleodepositional of carbonate source rock

Organofacies, particularly "carbonate organofacies", have been re-defined by Hartono et al. (2023) as carbonate rocks that have distinctive organic characteristics, which include the organic matter and factors that control the occurrence of organic matter itself, such as redox condition, mineralogy, and paleo-environment. Redox condition is one of the important substances in understanding the depositional environment, in which this study utilized framboidal pyrite morphology (Bond and Wignall, 2010; Blood et al., 2019) together with organic (Peters et al., 2005) and inorganic geochemical proxies (Algeo and Maynard, 2008; Wei and Algeo, 2020; Algeo and Li, 2020).

5.4.1 Framboidal pyrite

Framboidal pyrite morphology has been used to infer paleo-redox conditions (e.g., Bond and Wignall, 2010; Blood et al., 2019; Martizzi et al., 2021), in which the formation of this mineral is related to the fluctuation of the sulfide-oxidant transition zone, or later called chemocline boundary. Specifically, abundant, well-sorted, and small (<5 μm) framboidal pyrites have been interpreted to signify euxinic to anoxic sediments deposited beneath a chemocline high in the water column. On the other hand, Dysoxic conditions are represented by pyrite framboids with more varied diameters (6-10 μm, sub-ordinate larger framboids with framboids diameter size >10 μm) and poor sorting which suggests that the chemocline is situated near the sediment-water interface or in the sediment itself (Figure 14, Blood et al., 2019). Furthermore, under oxic conditions, the development of framboidal pyrite tends to be infrequent or entirely absent, primarily attributed to lower concentrations of sulfides present during deposition (Wilkin et al., 1996; Bond and Wignall, 2010; Blood et al., 2019).

The morphological disparities between these "mixed" shale facies already suggest distinct depositional conditions. In our investigation, the presence of well-sorted and finer framboidal pyrite observed in the Bule "mixed" shale (see Figure 15) suggests that the establishment of the chemocline occurred within the water column. This facies was consequently deposited in an environment characterized by higher sulfide content (anoxic condition), relative to the variably sized and poorly segregated framboids found in the Wiwi "mixed" shales. The latter observation indicates a suboxic environment and deposition near the chemocline.

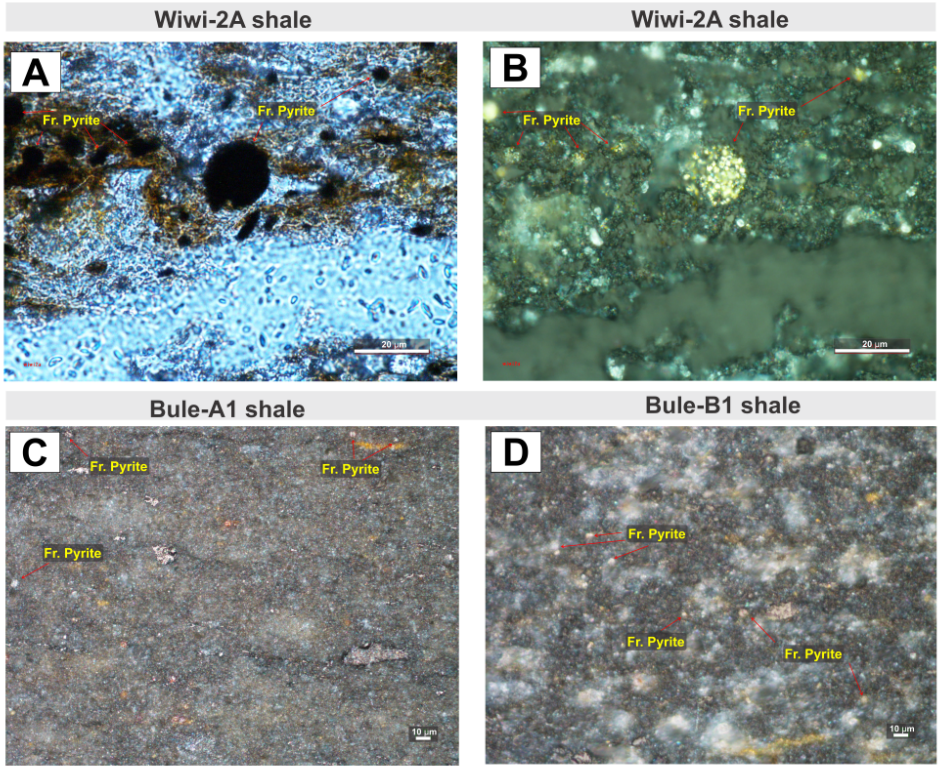

Figure 14. Photomicrographs of Wiwi and Bule "mixed" shales that show the differences in pyrite framboid morphologies. Wiwi shales contained poorly sorted and larger framboids (>10μm), followed by dispersed smaller framboids. Concurrently, Bule shale exhibited sparse, well-sorted, and smaller framboids below 5μm diameter. This morphological difference is related to the redox condition and chemocline position during shale deposition.

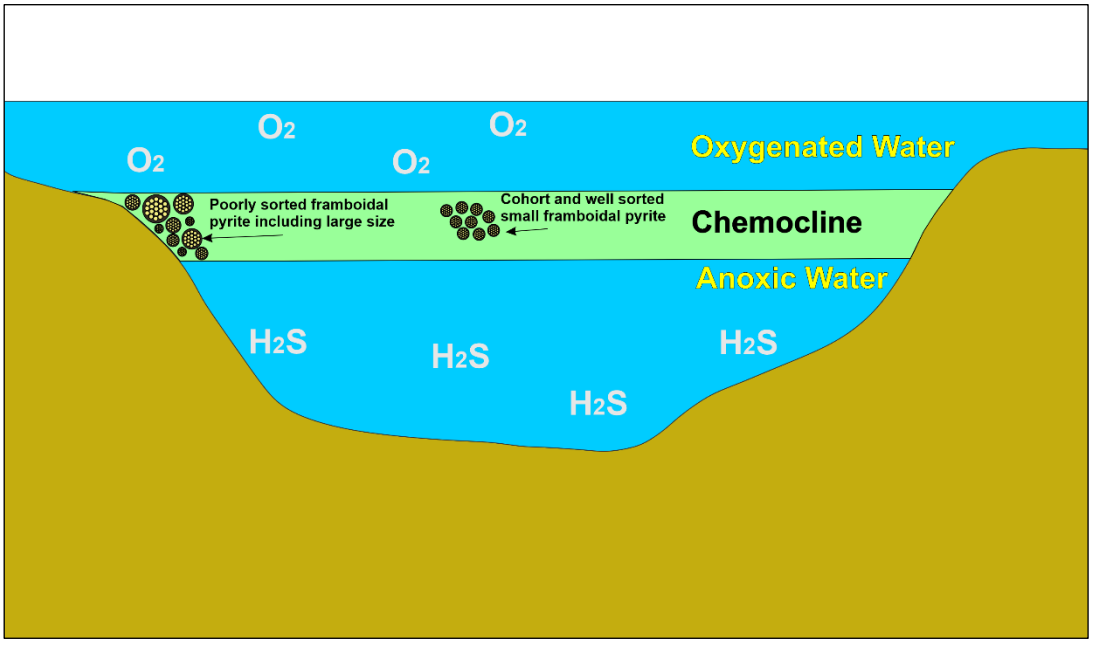

Figure 15. Illustration of chemocline boundary in relationship with framboidal pyrite morphology and distribution. The poorly sorted framboidal pytrite tend to indicate that chemocline boundary nearby the sediment-water interface where cohort and well sorted framboidal pyrite morphology indicating chemocline boundary located in water column (modified from Blood et al., 2019).

5.4.2 Elemental proxies

The redox conditions observed in the Wiwi and Bule "mixed" shales, along with the Matano argillaceous mudstone, were further corroborated by geochemical proxies (Table 4). Elemental ratio of vanadium (V), nickel (Ni), and chromium (Cr), typically denoted as V/(Ni+V) and V/Cr (Hatch and Leventhal, 1992; Jones and Manning, 1994; Gallaraga et al., 2008; Akinyemi et al., 2022), are common geochemical proxies to interpret redox condition in sedimentary environments. Under oxygen-depleted conditions, vanadium is more favorable to be preserved than nickel constituents (Algeo and Maynard, 2004; Galarraga et al., 2008). The V/(Ni+V) ratio of argillaceous mudstone of Matano Formations, respectively, indicating a dysoxic environment and oxic environment. In contrast, Wiwi "mixed" shale display V/(Ni+V) value suggesting a relatively suboxic to anoxic environment, where the Bule “mixed” shale indicating anoxic condition (Figure 16). On the other hand, the V/Cr ratio, is also giving a similar interpretation to all chemofacies (Figure 16). However, based on these parameters Wiwi “mixed” shale could be related to suboxic environment, while Bule “mixed” shale, further indicated anoxic environment, in-line with pyrite morphological observation (See table 1 for data summary).

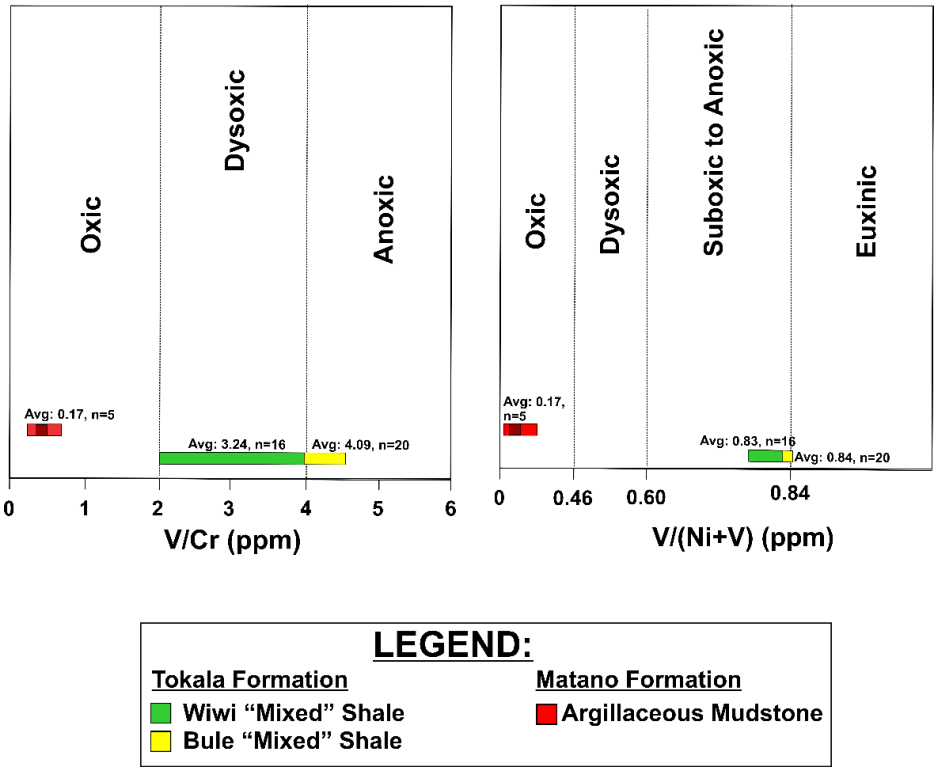

Figure 16. For paleoredox interpretation, trace element ratios such as the vanadium/chromium ratio (adapted from Jones and Manning, 1994) and vanadium/nickel ratio (adapted from Hatch and Leventhal, 1992) are utilized. The argillaceous mudstone of the Matano Formation displays strong oxic characteristics, as evidenced by these ratios. In contrast, the Wiwi and Bule "mixed" shales respectively exhibit dysoxic and anoxic conditions. Specifically, the Bule "mixed" shales tend to demonstrate a more pronounced anoxia compared to those observed in the Wiwi "mixed" shales.

5.4.3 Molecular proxies

The redox differences between Wiwi and Bule "mixed" shales were also recorded by molecular (biomarker) proxies. The Wiwi "mixed" shale exhibits a relatively high pristane/phytane (Pr/Ph) ratio and also C_{29} diahopanes peak is apparent (see supplementary data 2A), suggesting a suboxic environment (Didyk et al., 1978; Peters et al., 2005). Another specific proxy for redox interpretation is 28,30-bisnorhopanes, in which the origin of the compound is poorly understood. Peters et al. (2005) subjected this compound is related with an anoxic environment, while the compound was also recently found in a suboxic environment with a case from the Western India Offshore Basin. Therefore, we interpreted that the 28-30 bisnorhopanes found in the Wiwi "mixed" shale is also related to suboxic environment together with other suboxic biomarker parameters. On the other hand, Bule "mixed" shale has a relatively low Pr/Ph ratio and moderate C_{35}/C_{34} homohopanes ratio, supporting that the shale was deposited under anoxic conditions (Palacas et al., 1984; Peters et al., 2005). This redox discrepancy could be related to facies variation as carbonate-influenced facies tend to be more anoxic, whereas clay-rich facies was deposited under more oxic condition.

Carbonate influence during the deposition of Bule "mixed" shale is not just well-documented from petrography and elemental analyses but also notable in its biomarker composition. The 30-norhopanes series, which is typical on carbonate rock (Subroto et al., 1991), is apparent in the "mixed" shale facies of Bule sections together with other carbonate-related biomarker characteristics such as high Tm/Ts ratio and high C_{29}/C_{30} hopanes ratio (Table 3; Palacas et al., 1984; Peters et al., 2005). In Wiwi "mixed" shale facies, biomarker characteristics display relatively low C_{29}/C_{30} hopanes ratio with high diasteranes over steranes (see Supplementary Data 2A) indicating that the sediment was deposited in a more clastic environment with high clay-input (Peters et al., 2005).

Paleo-environment is also compulsory information to understand the organofacies. In general, "mixed" shale facies were deposited under marine environment suggested by the increasing pattern of C_{19}, C_{20}, and C_{21} tricyclic terpanes, dominant C_{23} tricyclic terpane, together with prominent peak of C_{24} tetracyclic terpane and C_{26} tricyclic terpane (Supplementary Data 2A; Price et al., 1987; Zumberge, 1987; Peters et al., 2005; Hartono et al., 2023). Shallow marine environment interpretation is also suggested by trifecta C_{27}-C_{28}-C_{29} steranes (Figure 17), but a slight difference was observed between the Wiwi and Bule "mixed" shales, in which Wiwi "mixed" shale tend to be enriched with C_{29} steranes. Similar observation was also recognized in the Seram Basin, where oils with high C_{29} sterane were interpreted to be derived from deep marine carbonate with diatom and radiolaria input (Hartono et al., 2023). Instead, the possibility of deep marine carbonate deposition, we believed that high C_{29} sterane

in the Wiwi "mixed" shale still related to terrestrial OM (Huang and Meinschein, 1979) as such OM was frequent under petrographic observation (Figure 5D and 5E) Consequently, both Wiwi and Bule "mixed" shales were interpreted to be deposited in a much shallower environment compared to those Triassic carbonates in the Seram Basin. Confirming this argument, biomarker proxies utilized by Hartono et al. (2021) in the Seram Basin, such as C_{24}/C_{23} tricyclic terpanes, C_{26}/C_{25} tricyclic terpanes, C_{27}/C_{29} steranes, and hopanes/steranes ratio, suggests that our samples were indeed part of "shelf edges carbonate" environment (term from Palacas et al., 1984). The shelf edge carbonate term is also applicable for both carbonates as a previous geological study did mention that the Tokala Formation was a shelfal carbonate platform (Surono and Hartono, 2013). Furthermore, these shallow marine carbonate facies could be further divided from their redox condition, water depth, and depositional energy in this study with a case from bule and Wiwi "mixed" shale by modifying classification from Hartono et al. (2021). More proximal Wiwi "mixed" shale exhibits lower hopanes/steranes and higher C_{24}/C_{23} tricyclic terpanes ratio, in contrast to more distal and anoxic Bule "mixed" shale.

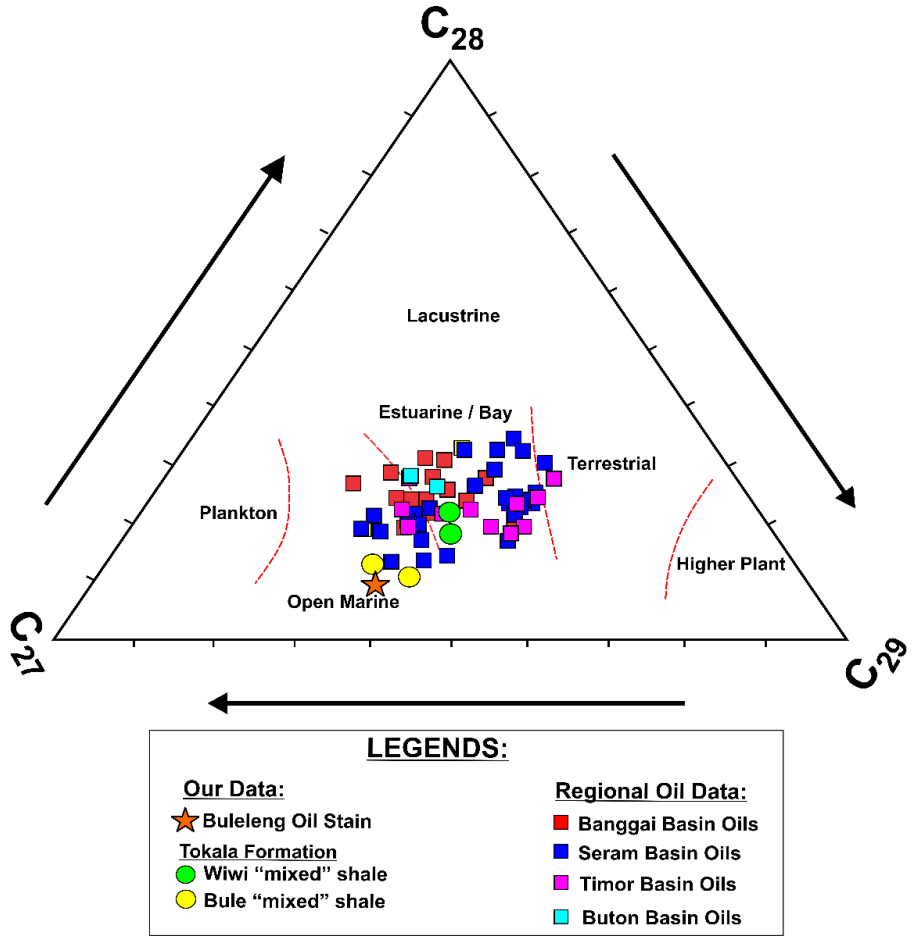

Figure 17. Ternary plot of C_{27}, C_{28}, and C_{29} steranes (background from Huang and Meinschein, 1979) for paleoenvironment determination. Bule "mixed" shales tend to have higher C27 sterane that might relate to a more marine (distal) environment, while Wiwi "mixed" shales have relatively similar C_{27} and C_{29} steranes indicating a transitional environment. Compared to other eastern Indonesia oils (Bintuni oils, Dolan and Hermany, 1988; Subroto and Sapiie, 2014;

Banggai oils Satyana and Zaitun, 2016; Timor oils, Setyowati et al., 2022; Seram oils Hartono et al., 2023; Buton Oils, Tobing, 2008), Bule oil and "mixed" shales have identical characteristic with Seram oils regionally.

In this study, a multi-proxy approach was employed to elucidate the paleo-redox conditions and depositional environments of the Wiwi and Bule "mixed" shale units. Through integrated analysis of pyrite framboid size and morphology, elemental geochemistry, and organic molecular parameter signatures, we effectively constrained the paleo-redox conditions and depositional characteristics of the investigated intervals.

5.5 New model for syn-rift carbonate source rock deposition

Direct observation has given us a preliminary hint about the depositional facies variation in the marine carbonate environment of the Tokala Formation. This variation was then simplified into two major chemofacies, such as argillaceous and "mixed" shale facies, representing sedimentological processes from source-to-sink. Comprehensive inorganic and organic geochemical approaches suggested that mixed facies were shelf carbonate platform deposits that, at least, consisted of two types of carbonates organofacies (terms from Palacas et al., 1984; Hartono et al., 2023), referred to as Wiwi and Bule "mixed" shales. Bule "mixed" shale tends to be richer in carbonate content and deposited in more marine-prone areas that exhibit anoxic and stable (low clay input) conditions with dominant marine algae input and homogenous organisms. In contrast, Wiwi "mixed" shale was deposited in the more proximal area with diverse organisms under more oxic-suboxic and high-energy conditions with a relatively higher percentage of terrestrial organic matter compared to marine algae. The interpretation from field-to-elemental-and-molecular scales was then integrated with the regional geology of Southeast Sulawesi (Rusmana et al., 1993; Surono and Bachri, 2002; Nugraha and Hall, 2018, 2022) and also geological concept to propose a new depositional model of syn-rift carbonate source rock. We put two important aspects of how carbonate source rock was formed, which are tectonic (in this case extensional tectonic; Spakman and Hall, 2010; Rudyawan and Hall, 2012; Surono and Hartono, 2013; Nugraha and Hall, 2022) and sedimentological aspect, especially detrital input and carbonate development (Figure 18). First, the earliest basin fill was initiated with the deposition of alluvial fan (talus) near the border fault (Gawthorpe and Leeder, 1998), while detrital sediment (quartz and clay minerals) was supplied from Gondwana in the south. It also should be noted that the fluvial system carried oxygen to the sea (Figure 18) that which affect organic matter preservation. This terrestrial-fluvio-deltaic deposits is represented by the Meluhu Formation composed of sandstone, coal, and siltstone (Rusmana et al., 1993a; Surono, 1994; Surono and Bachri, 2002) and later the deposition was followed by marine incursion.

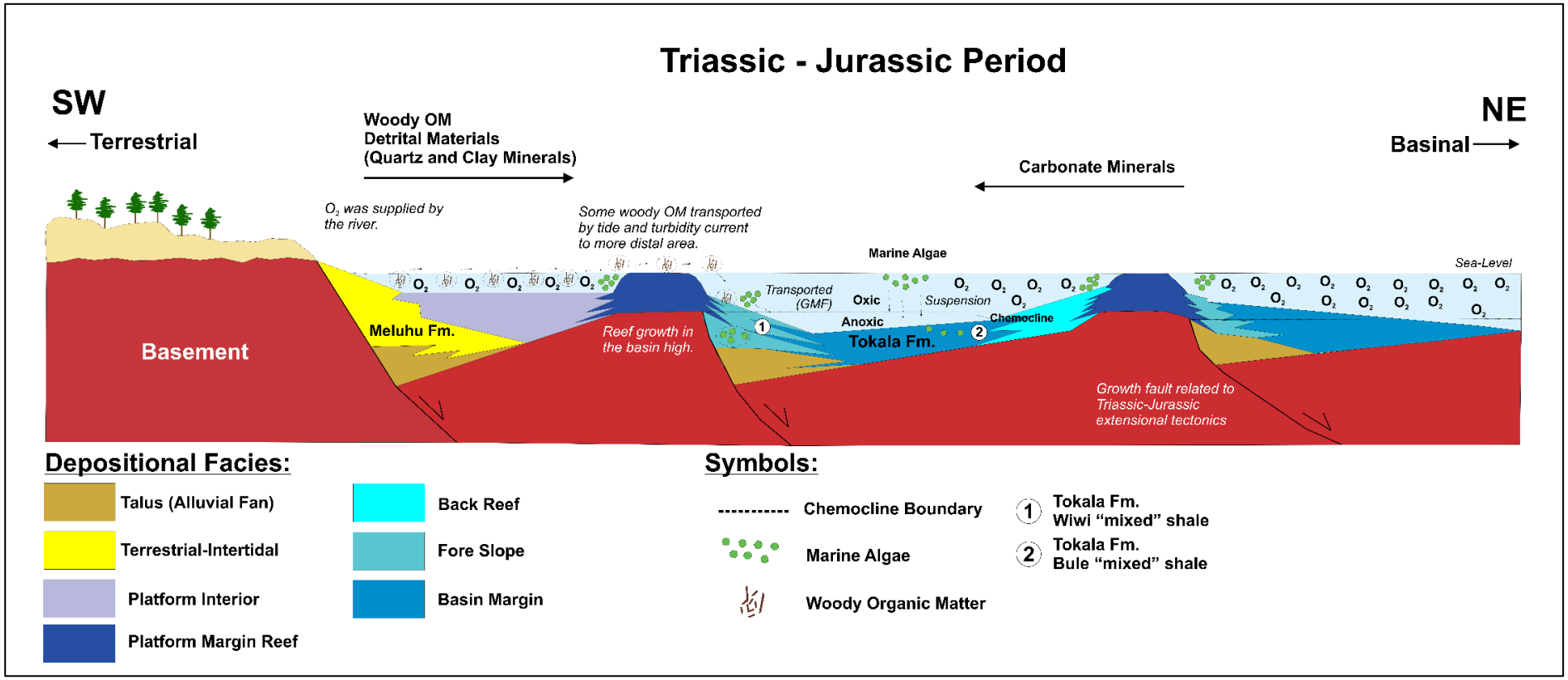

Figure 18. Proposed new schematic depositional model and organic matter enrichment mechanism on syn-rift carbonate source rock based on the integration of field-to-elemental-and-molecular observation and regional geology. Two important aspects in our model are tectonic and sedimentological aspect, especially detrital input and carbonate development. In our model, sedimentation processes occurred in two fashions, such as suspension and gravity mass movement, resulting in organic matter accumulation. The classical concept of organic matter accumulation could be seen in the basin margin (Bule "mixed" shale facies), where suspended organic matter was then preserved under the anoxic bottom of water. Another strong novelty from our model is that the triggered gravity mass flow from margin reef facies due to fault activities resulted in rapid sedimentation so that the organic matter was well-preserved in the fore slope facies (Wiwi "mixed" shale facies).

Moreover, in response to the marine incursion, far distal from the continental source, carbonate reef, a source of carbonate materials, developed in the basin high (Figure 18) due to carbonate reefs need shallow, warm, and clear conditions to grow (Tucker et al., 1993). Adapting facies model from Nichols (2009) and Flugel (2010), the carbonate reef further growth into a carbonate platform that could be divided into platform interior, platform margin reef, back reef, and fore reef facies (Figure 18). Fluvio-deltaic deposition, however, still continued in more proximal areas, supplying terrestrial sediment and organic matter to the basin. This delta-carbonate platform depositional style in the horst-graben setting itself is common, for example, in the Kutai Basin (Indonesia; Moss and Chambers, 1999). In terms of organic matter, oxygenated water, or euphotic zone, around the platform margin reef exhibits a suitable environment for marine algae and plankton. The deceased marine algae were then suspended to the basin margin and preserved under anoxic conditions. We place the boundary of oxic and anoxic below the platform margin facies where it is believed that coral reefs could not be developed without oxygen and sunlight (Tucker et al., 1993). Another compelling argument is the occurrence of chemocline boundary which separates the sulfide-bearing water with oxygenated water (Figure 18; Blood et al., 2019) that was observed from framboidal morphological distribution. Hence, Tokala Formation in the Bule section has a good quantity and quality of organic matter due to excellent preservation. Different case with Bule "mixed" shale, another sedimentation mechanism outside suspension could probably control the organic enrichment in Wiwi "mixed" shale, which became our strong point in the syn-rift carbonate source rock model. Numerous studies have discussed the organic enrichment in a carbonate environment together with its capability to act as source rocks (Xia et al., 2019), but syn-extensional fault controls on the source rock formation are rarely discussed. Syn-extensional faults arise as a consequence of syn-rift tectonics, triggering gravitational mass flow (GMF) processes (Dorobek, 2008; Masiero et al., 2021) that facilitate the accumulation of calci-turbidites. Nugroho et al. (2009) provide a compelling analog of the carbonate turbidite system in the Oligo-Miocene Rajamandala carbonate in West Java, in which calci-turbidite was poured in front of the platform margin reef. Our research observed that Wiwi "mixed" shale is part of the carbonate turbidite system, as shown by the presence of low-angle contorted structures. (Figure 4A). This GMF triggered by fault activity is crucial for organic matter preservation in the Wiwi "mixed" shale, despite oxic to suboxic condition as suggested by biomarker and elemental analyses. To achieve excellent preservation, while the condition was oxic, a high sedimentation rate is needed (Dembicki Jr., 2017) and, in our case, was provided by the GMF (Figure 18).

One intriguing aspect of our model is the occurrence of a significant concentration of woody OM in the carbonate environment (Figure 5H and 5K), specifically in the fore slope facies of Wiwi "mixed" shale. The plausible mechanism for this case is that the wood fragments were transported further into the carbonate platform by a turbidite system related to the delta system in the south (Figure 18). Omura and Hoyanagi (2004) also observed the terrigenous OM were transported into the basinal area during the transgressive stage. Another evidence was also brought by Ekweozor and Telnaes (1990), in which a terrestrial-derived biomarker (oleanane) was also discovered in deep marine sediments of the Niger Delta, interpreted to be carried by turbidite system.

5.6 Challenges for our model: regional and global comparison

This study gives a big picture regarding the term "carbonate source rock" which is actually not fully composed of carbonate minerals but rather a mixture of carbonate and siliciclastic materials, in which the counterpoise between these contents reflects the depositional condition that controls organic matter enrichment. Moreover, we have also explained the organic matter depositional mechanism in the carbonate environment inferred from multiple proxies, which consequently proved that even one carbonate platform could consist of at least two organofacies. Previously, Hartono et al. (2023) provided a good separation of two oil subfamilies that have long been considered one family as carbonate-derived oil. However, the mechanism responsible for this distinction on organofacies, even direct discrimination on the source organofacies itself, is still poorly documented. Here, two organofacies were recognized, such as the most common organofacies that act as "carbonate source rock", basin margin facies (e.g., Seram Basin, Hartono et al., 2023), and our new proposed one, fore slope facies. As predicted, Bule oil-stain exhibits typical carbonate biomarker characteristics so that this hydrocarbon is strongly correlated with the basin margin facies. The derivative of fore slope facies is still enigmatic as the facies display good source rock capability. Furthermore, a comparison with other regional and global carbonate source rocks was done to challenge our model.

Triassic-Jurassic carbonate source rocks are widely distributed in eastern Indonesia, for example, Saman-Saman and Manusela Formations (Seram Basin, Hartono et al., 2023), Winto Formation (Buton Basin, Satyana, 2013), and Aitutu Formation (Timor Basin, Permana et al., 2014). For regional comparison, a recent geochemical study of Seram oils suggested that the carbonate source rock in the Seram Basin could be further divided into deep and shallow marine carbonate which have distinct types of organic matter (Hartono et al., 2021, 2023) and even this finding might apply to other Triassic eastern Indonesia carbonates. One problem that still exists is that these probable organofacies have not been found in surface and subsurface so no

successful direct oil correlation has ever been done. This problem is probably caused by the lack of knowledge on the description of carbonate source rock. Our model answered the poor description related to carbonate source rock in Seram, and even further eastern Indonesia. First, the C_{27}-C_{28}- C_{29} steranes plot indicated that Bule oil, derived from Tokala shale, shares similarities with Seram oils (Figure 17). It is also confirmed with other biomarker fingerprints that Seram shallow marine carbonate oils (Family B in Hartono et al., 2023) matched our Tokala basin margin facies. In addition, the predominance of C_{29} steranes in Wiwi "mixed" shale is not related to the deep marine diatom and radiolaria, as suggested by Hartono et al. (2023), but rather related to terrestrial organic matter since we found woody OM in Wiwi "mixed" shale (Huang and Meinschein, 1979). Well, the interpretation of the origin of C_{29} steranes, diatom origin in Seram (Hartono et al., 2023), and terrestrial origin in Wiwi "mixed" shale, is both correct as the paleo-geography of Southeast-arm Sulawasi was relatively near the sediment source (Surono and Hartono, 2013; Nugraha and Hall, 2022), while Seram Basin was more distant from the continent.

In a global manner, carbonate-associated source rock has been studied in petroliferous basins such as Mesozoic La Luna Formation in Magdalena Basin (Colombia; Zumberge, 1984; Rangel et al., 2000; Mongenot et al., 2016), Smackover Formation (Gulf of Mexico; Oehler, 1984), and Sargelu Formation in Zagros area (Southwestern Asia; Al-Ameri et al., 2014; Abdula, 2015; Hakimi and Najaf, 2016; Hakimi et al., 2018; Tobia et al., 2019). Carbonate source rock is defined globally as organic-rich sedimentary rock comprising at least 50% carbonate minerals, but also fit to layer containing less than 50% carbonate yet still substantial amounts or marl (Palacas et al., 1984). Our data shows that too much carbonate content, the limestone group with 50% CaO, contrastingly with the definition, displays low TOC and PY. Previously, Xia et al. (2019 and references therein) already separated the threshold for carbonate source rock which is lower from shale. However, we disagree with the different classifications for shale and carbonate source rock as source rock must acquire a good quantity of organic matter apart from its mineralogies. It is also confirmed by several productive unconventional shale reservoirs with various mineralogical content in the US that display high TOC and HI (Jarvie et al., 2012; Mews et al., 2019). Hence, based on our observation, the global term carbonate source rock is more suitable for our "mixed" shale which is composed of considerable carbonate and siliceous content.

To be specific, our model is compared to the world-class carbonate source rock, the Jurassic Sargelu Formation, as it shares similar genetics which is an organic-rich carbonate deposited during the rifting event (Bordenave and Burwood, 1990; Hakimi and Najaf, 2016). Sargelu Formation contained is dominantly composed of oil-prone kerogen, as evidenced by

high HI ranging from 222 to 727 (Al-Ameri et al., 2014; Abdula, 2015; Hakimi and Najaf, 2016). Moreover, data from Tobia et al. (2019) shows that the formation is composed of SiO_2 (8.56-33.3%) and CaO (12.95-41.9%) which is within our "mixed" shale spectrum. This comparison confirmed that the carbonate source rock was actually formed by the mixture of carbonate and siliciclastic constituents. Furthermore, Bule "mixed" shale exhibits similar biomarker characteristics with Sargelu source rock (Hakimi and Najaf, 2016), in which the productive interval could be assigned as basin margin facies from our model. This implies that organic matter enrichment in a carbonate environment is strongly controlled by stable organic matter deposition preserved by anoxic bottom of water. Despite that, referring to our model, further possibilities to explore the fore slope facies in the Sargelu Formation are widely open. Since the formation is a syn-extensional deposit, active tectonic activities triggered gravity-style transportation from the carbonate reef resulting in organic-matter accumulation.

Chapter VI: CONCLUSIONS

To summarize, our study re-defined the term "carbonate source rock" to denote a mixture of carbonate and siliciclastic materials, not strictly carbonate minerals alone, where the proportion of these constituents is related to the depositional environment in control of organic matter accumulation. Additionally, two potential organofacies mechanisms in the carbonate environment are discovered, inferred from observing multiple proxies: basin margin-associated facies and fore slope facies, in which our evidence demonstrated that these two facies could consist in a single carbonate platform. Moreover, we develop a new integrated depositional model, capturing the interplay between sedimentation, diagenesis, and basinal evolution under syn-rift tectonic regimes. Our depositional model, shows two primary sedimentation mechanisms, in which suspension settling and gravity-driven mass transport influenced organic matter sequestration. Through these depositional pathways, organic carbon was delivered and concentrated to facilitate the formation of potential hydrocarbon source facies. This new model integrated the understanding of global "carbonate source rock" and might be applicable across the regional and global scales on similar syn-extensional carbonate petroleum.

REFERENCES

Abdula, R. A., 2015. Hydrocarbon potential of Sargelu Formation and oil-source correlation, Iraqi Kurdistan. Arabian Journal of Geosciences 8(8), 5845–5868.

Advokaat, E. L., van Hinsbergen, D. J. J., 2023. Finding Argoland: Reconstructing a microcontinental archipelago from the SE Asian accretionary orogen, Gondwana Research 128, 161–263, https://doi.org/10.1016/j.gr.2023.10.005

Akinyemi, S. A. Adebayo, O. F., Madukwe, H. Y., Kayode, A. T., Aturamu, A. O., OlaOlorun, O. A., Nyakuma, B. B., Jauro, A., Gitari, W. M., Mudzielwana, R., Hower, J. C., 2022. Elemental geochemistry and organic facies of selected cretaceous coals from the Benue Trough basin in Nigeria: Implication for paleodepositional environments. Marine and Petroleum Geology 137,105490. https://doi.org/10.1016/j.marpetgeo.2021.105490.

Allen, P.A., Allen, J.R., 2013. Basin Analysis-Principles and Application to Petroleum Play Assessment. Third Edition, Wiley and Blackwell, Hoboken.

Algeo, T.J., Maynard, J.B., 2004. Trace-Element Behavior and Redox Facies in Core Shales of Upper Pennsylvanian Kansas-Type Cyclothems. Chemical Geology, 206, 289-318. https://doi.org/10.1016/j.chemgeo.2003.12.009

Algeo, T. J., Li, C., 2019. Redox classification and calibration of redox threshold in sedimentary systems. Geocjhimica et Comochimica Acta, 287, 8–12.

Algeo, T. J., Liu, J., 2020. A re-assessment of elemental proxies for paleoredox analysis. Chemical Geology, 540. https://doi.org/10.1016/j.chemgeo.2020.119549

Al-Ameri, T. K., Najaf, A. A., Al-Khafaji, A. S., 2014. Hydrocarbon potential of the Sargelu Formation, North Iraq. 7(3), 987–1000. doi:10.1007/s12517-013-0875-8

Ando, T., Sawada, K., Okano, K., Takashima, R., Nishi, H., 2017a. Marine primary producer community during the mid-Cretaceous oceanic anoxic events (OAEs) 1a, 1b and 1d in the Vocontian Basin (SE France) evaluated from triaromatic steroids in sediments. Org. Geochem, 106, 13–24. https://doi.org/10.1016/j.orggeochem.2017.02.002

Ando, T., Sawada, K., Nakamura, H., Omatsu, K., Takashima, R., Nishi, H., 2017b. Depositional environments and maturity evaluated by biomarker analyses of sediments deposited across the Cenomanian–Turonian boundary in the Yezo Group, Tomamae area, Hokkaido, Japan. Island Arc 26, 12178. https://doi.org/10.1111/iar.12178.

Ando, T., Sawada, K., Okano, K., Takashima, R., & Nishi, H. (2022). Marine paleoecological variations during the mid-Cretaceous oceanic anoxic event 1a in the Vocontian Basin, southeastern France. *Palaeogeography, Palaeoclimatology, Palaeoecology*, *586*. https://doi.org/10.1016/j.palaeo.2021.110779

Audley-Charles, M.G., Carter, D.J., Barber, A.J., Norvick, M.S., Tjokrosapoetro, S., 1979. Reinterpretation of the geology of Seram: implications for the Banda Arcs and northern Australia. Journal Geological Society of London 136, 547–568

Behar, F., Beaumont, V., De, B., Penteado, H. L., 2001. Rock-Eval 6 technology: Performances and developments. Oil & gas Science and Technology. Revue de l'Institut Francais du Petrole, 56, 111–134.

Blood, D. R., Schlagle, S., Hefferan, C. M., Vazquez, A., McAlister, D., 2019. Diagenetic pyrite morphology in mudstiones of the Upper Ordovivian Point Pleasant limestone, appalachan Basin: evidence for dysoxic deposition. AAPG Memoir 120, 69–82.

Bond, D.P.G., and Wignall, P.B., 2010, Pyrite framboid study of marine Permian-Triassic boundary sections: A complex anoxic event and its relationship to contemporaneous mass extinction: Geological Society of America Bulletin, 122, 1265–1279, doi:10.1130/B30042.1

Bordenave, M. L., Burwood, R., 1990. Source rock distribution and maturation in the Zagros Orogenic Belt: Provenance of the Asmari and Bangestan Reservoir oil accumulations, Organic Geochemistry 16 (1–3), 369–387. https://doi.org/10.1016/0146-6380(90)90055-5.

Bordenave, M. L., 1993. Applied petroleum geochemistry. Editions Technip, 524 p.

Bruce S. H., Michael H. H., 2022. Revisiting paleoenvironmental analyses and interpretations of organic-rich deposits: The importance of TOC corrections. Organic Geochemistry, 170, 104434. https://doi.org/10.1016/j.orggeochem.2022.104434.

Burhanuddin, M.S., Subroto, E. A., Santy, L. D., Susanto, V., Fahruddin, A., 2020. Geochemistry Characterization of Oil and Source Rock in Southern Tomori Basin. The 5th International Conference of Geology (ICGEF 2020). 23

Davidson, J. W., 1991. *The Geology and Prospectivity of Buton Island, S.E. Sulawesi, Indonesia*.

Demaison, G.J. Moore, G.T., 1980. Anoxic Environments and Oil Source Rock Bed Genesis. American Association of Petroleum Geologists Bulletin, 64, 1179-1209.

Dembicki Jr., H., 2009. Three common source rock evaluation errors made by geologists during prospect or play appraisals. American Association of Petroleum Geologists Bulletin, 93, 341-356. https://doi.org/10.1306/10230808076

Dembicki Jr., H., 2017. Practical petroleum geochemistry for exploration and production. Elsevier, 331 p.

Dickinson, W.R., 1985. Interpreting Provenance Relations from Detrital Modes of Sandstones. In: Zuffa, G.C., Ed., Provenance of Arenites. D. Reidel Publishing Company. Dordrecht, The Netherlands, 333-362. https://doi.org/10.1007/978-94-017-2809-6_15

Didyk, B., Simoneit, B., Brassell, S., Eglinton, G., 1978. Organic geochemical indicators of palaeoenvironmental conditions of sedimentation. Nature, **272**, 216–222. https://doi.org/10.1038/272216a0

Dorobek, S., 2008. Tectonic and Depositional Controls on Syn-Rift Carbonate Platform Sedimentation, In: Lukasik, J., Simo, J. A. T. (Ed.), Controls on Carbonate Platform and Reef Development. SEPM Society for Sedimentary Geology Special Publication 89. https://doi.org/10.2110/pec.08.89.0057

Ekweozor, C. M., Telnaes, N., 1990. Oleanane parameter: Verification by quantitative study of the biomarker occurrence in sediments of the Niger delta. Organic Geochemistry 16 (1–3), 401–413. https://doi.org/10.1016/0146-6380(90)90057-7.

Flugel, E., 2010. Microfacies of Carbonate Rocks, Analysis, Interpretation and Application. Springer-Verlag, Berlin, 976 p.

Galarraga, F., Reategui, K., Martïnez, A., Martínez, M., Llamas, J. F., Márquez, G., 2008. V/Ni ratio as a parameter in palaeoenvironmental characterisation of nonmature medium-crude oils from several Latin American basins. Journal of Petroleum Science and Engineering, 61(1), 9–14. https://doi.org/10.1016/j.petrol.2007.10.001

Gamero-Diaz H, Miller CK, Lewis R., 2013. sCore: a mineralogy-based classification scheme for organic mudstones. In: SPE Annual Technical Conference and Exhibition. https://doi.org/10.2118/166284-MS

Gawthorpe, R. L. and Leeder, M. R., 2000. Tectono-sedimentary evolution of active extensional basins. Basin Research, 12, 195–218. https://doi.org/10.1111/j.1365-2117.2000.00121.x

Hakimi, M. H., Najaf, A. A., 2016. Origin of crude oils from oilfields in the Zagros Fold Belt, southern Iraq: Relation to organic matter input and paleoenvironmental conditions. *Marine and Petroleum Geology*, *78*, 547–561. https://doi.org/10.1016/j.marpetgeo.2016.10.012

Hakimi, M. H., Najaf, A. A., Abdula, R. A., Mohialdeen, I. M. J., 2018. Generation and expulsion history of oil-source rock (Middle Jurassic Sargelu Formation) in the Kurdistan of north Iraq, Zagros folded belt: Implications from 1D basin modeling study. Journal of Petroleum Science and Engineering 162, 852–872. https://doi.org/10.1016/j.petrol.2017.11.013.

Hartono, B. M., Subroto, E. A., Kesumajana, A. H. P., Andrianto, R., Malvinas, G., Wahyudiono, J., 2023. Geochemistry of carbonate-derived oils in the Seram Basin, eastern Indonesia: A new hydrocarbon generation, migration, and preservation model for exploration in fold-thrust belts. Journal of Asian Earth Sciences, 250. https://doi.org/10.1016/j.jseaes.2023.105647

Hartono, B.M., Subroto, E.A., Kesumajana, A.H.P., Andrianto, R., Wahyudiono, J., Malvinas, G., Priyanto, B., 2022. New interpretation of the nature and origin of carbonate-derived oil in Seram Basin, eastern Indonesia. IOP Conference Series: Earth and Environmental Science 1047, 012032.

Hartono, B. M., Subroto, E. A., Kesumajana, A. H. P., Andrianto, R., Malvinas, G., Wahyudiono, J., & Priyanto, B., 2021. New Interpretation of The Nature and Origin of Carbonate-derived Oil in Seram Basin, Eastern Indonesia.

Hatch, J., Leventhal, J., 1992. Relationship between inferred redox potential of the depositional environment and geochemistry of the upper Pennsylvanian (missourian) Stark shale member of the Dennis limestone, wabaunsee county, Kansas, USA. Chemical Geology 99 (1–3), 65–82.

Herron, M., 1998. Geochemical classification of terrigenous sands and shales from core or log data. Journal of Sedimentary Research 58 (5). http://dx.doi.org/10.1306/212F8E77-2B24-11D7-8648000102C1865D

Huang, W. Y. dan Meinschein, W. G., 1979. Sterols as ecological indicators, Geochimica et Cosmochimica Acta 43**,** 739–745.

Hughes, W.B., 1984. Use of thiophenic organosulfur compounds in characterizing crude oils derived from carbonate versus siliciclastic sources. In: Palacas, J.G. (Ed.), Petroleum

Geochemistry and Source Rock Potential of Carbonate Rocks. American Association of Petroleum Geologists, Tulsa, Oklahoma, pp. 181–196.

Hutton, A.C., Cook, A.C., 1980. Influence of alginite on the reflectance of vitrinite from Joadja, NSW, and some other coals and oil shales containing alginite. Fuel 59 (10), 711–714. https://doi.org/10.1016/0016-2361(80)90025-3

Hunt, J. M., 1996. Petroleum Geochemistry and Geology, second ed. Freeman and Company, New York, p 743P.

Hurst, A., 1986. Sandstone Reservoir Description: An Overview of the Role of Geology and Mineralogy. Clay Minerals, 21 (4), 791-809. 10.1180/claymin.1986.021.4.21

Jarvie, et al., 2007. Unconventional Shale Gas System: The Mississippian Barnet Shale of North-Central Texas as One Model for Thermogenic Shale Gas Assessment. AAPG Bulletin 91, 475–499. https://doi.org/10.1306/12190606068

Jarvie, D. M., 2012. Shale resource systems for oil and gas: part 1—Shale-gas resource systems, In: J.A. Breyer (Ed.), Shale Reservoirs—Giant Resources for the 21st century. AAPG Memoir 97, pp. 69–87.

Jiyang, S., Benshan, W., Lijie, Z., Zhiqing, H., 1988. Study on diagenesis of organic matter in immature rocks. Organic Geochemistry,13 (4–6), 869-874, https://doi.org/10.1016/0146-6380(88)90239-2.

Jones, B., Manning, D.A., 1994. Comparison of geochemical indices used for the interpretation of palaeoredox conditions in ancient mudstones. Chem. Geol. 111 (1–4), 111–129.

Kemp, G., Mogg. W., 1992. A Re-Appraisal of The Geology, Tectonics, and Prospectivity of Seram Island, Eastern Indonesia, Annual Convention of Indonesian Petroleum Association, 521–551.

Kurniawan, A. P., Mardianza, A., Firman, I., Fajar, M., 2019. New biomarker evidences of Mesozoic petroleum system in the unexplored Tokala area, Eastern Sulawesi. Proceedings, Indonesian Petroleum Association. Forty-Third Annual Convention & Exhibition. IPA19-G-350.

Lafargue, E., Espitali´e, J., Marquis, F., Pillot, D., 1998. Rock-Eval 6 applications in hydrocarbon exploration, production and in soil contamination studies. Rev. Inst. Fr. Petrol 53, 421–437.

Livsey, A. R., Duxbury, N., Richards, F., 1992. The Geochemistry of Tertiary and Pre-Tertiary Source Rocks and Associated Oils in Eastern Indonesia.

Masiero, I., Burgess, P., Hollis, C., Manifold, L., Gawthorpe, R., Lecomte, I., Marshall, J., Rotevatn, A., 2021. Syn-rift carbonate platforms in space and time: testing and refining conceptual models using stratigraphic and seismic numerical forward modelling. Geological Society of London Special Publication 509, pp. 179–203. 10.1144/SP509-2019-217.

Martizzi, P., Chiyonobu, S., Hibi, Y., Yamato, H., Arato, H., 2021. Middle–late Miocene paleoenvironment of the Japan sea inferred by sedimentological and geochemical characterization of coeval sedimentary rocks. Marine and Petroleum Geology, 128, https://doi.org/10.1016/j.marpetgeo.2021.105059.

Mews, K. S., Alhubail, M. M., Barati, R. G., 2019. A review of brittleness index correlations for unconventional tight and ultra-tight reservoirs. Geosciences *9* (7), 319.

Moss, S., Chambers, J. L. C., 1999. Tertiary facies architecture in the Kutai Basin, Kalimantan, Indonesia. Journal of Asian Earth Sciences 17 (1), 157–181. 10.1016/S0743-9547(98)00035-X

Nichols, G., 2009. Sedimentology and Stratigraphy. Blackwell Science Ltd., London, 335 p.

Nugraha, A. M. S., Hall, R., Late Cenozoic palaeogeography of Sulawesi, Indonesia, Palaeogeography, Palaeoclimatology, Palaeoecology 490, 191–209. https://doi.org/10.1016/j.palaeo.2017.10.033.

Nugraha, A. M. S., Hall, R., 2022. Neogene sediment provenance and paleogeography of SE Sulawesi, Indonesia. Basin Research 34 (5), 1714–1730. https://doi.org/10.1111/bre.12682

Dwiharso Nugroho, Simo, T., Noeradi, D., Fullmer, S. M., Hicks, m. K., Kaczmarek, S. E., Liu, C., Van Gorsel, J. T., Steffen, K., Ruf, A., Sapiie, B., Terrell, M., Saikia, I., 2009. Significance of the sedimentology and stratigraphy for the evolution and demise of the Oligocene Rajamandala limestone, Padalarang, West Java, Indonesia. Proceedings, Indonesian Petroleum Association, Thirty-Third Annual Convention & Exhibition, IPA09-G-161.

Noble, R., Orange, D., Decker, J., Teas, P., Baillie, P., 2009. Oil and Gas Seep in Deep Marine Sea Floor Cores as Indicators of Active Petroleum Systems in Indonesia.

North, F. K., (1990). Petroleum Geology. Unwin Hyman. ISBN 10: 0045530041 / ISBN 13: 9780045530045

McKinley, J.M., Worden, R.H., Ruffell, A.H., 2003. Smectite in Sandstones: a review of the controls on occurrence and behaviour during diagenesis. In: Worden, R.H., Morad, S. (Eds.), Clay Mineral Cements in Sandstones, vol. 34. International Association of Sedimentologists. Special Publication, pp. 109–128.

Meyers, P. A., 1997. Organic geochemical proxies of paleoceanographic, paleolimnologic, and paleoclimatic processes. Organic Geochemistry 27(5–6), 213–250. DOI: https://doi.org/10.1016/S0146-6380(97)00049-1

Molenaar, N., Vaznytė, J., Bär, K., Šliaupa, S., 2021. Illite and chlorite cementation of siliciclastic sandstones influenced by clay grain cutans. Marine and Petroleum Geology, 132,105234. https://doi.org/10.1016/j.marpetgeo.2021.105234.

Mongenot, T., Tribovillard, N., Desprairies, A., Lallier-Vergès, E., Laggoun-Defarge, F., 2016. Trace elements as palaeoenvironmental markers in strongly mature hydrocarbon source rocks: the Cretaceous La Luna Formation of Venezuela. Sedimentary Geology 103(1–2), 23–37. https://doi.org/10.1016/0037-0738(95)00078-X.

Oehler, J. H., 1984. Carbonate Source Rock in The Jurassic Samckover Trend, Mississipi, Alabama, and Florida. AAPG Studies in Geology 18, 63–69.

Omura, A., Hoyanagi, K., 2004. Relationships Between Composition of Organic Matter, Depositional Environments, and Sea-Level Changes in Backarc Basins, Central Japan. Journal of Sedimentary Research 74, 620–630.

Palacas, J. G., Anders, D. E., King, J. D., 1984. South Florida Basin-Prime Example of Carbonate Source Rocks of Petroleum. AAPG Studies in Geology, 71–96.

Passey, Q. R., Bohacs, K. M., Esch, W. L., Klimentidis, R., Sinha, S., 2010. From oil-prone source rock to gas-producing shale reservoir–Geological and petrophysical characterization of unconventional shale-gas reservoirs. In International oil and gas conference and exhibition in China. Society of Petroleum Engineers. https://doi.org/10.2118/131350-MS

Permana, A. K., Kusworo, A., Prastian, A. H., 2014. Characteristics of the Triassic Source Rocks of the Aitutu Formation in the (West) Timor Basin. *Indonesian Journal on Geoscience* 1(3), 165–174, 10.17014/ijog.1.3.165-174.

Peters, K.E., 1986. Guidelines for Evaluating Petroleum Source Rock Using Programmed Pyrolysis. American Association of Petroleum Geologists Bulletin 70, 318–329.

Peters, K. E., Moldowan, J. M., 1993. The Biomarker Guide: Interpreting Molecular Fossils in Petroleum and Ancient Sediments. Prentice Hall.

Peters, K.E., Cassa, M.R., 1994. Applied source-rock geochemistry. In: Magoon, L.B., Dow, W.G., Eds., The petroleum system: from source to trap, American Association of Petroleum Geologists, Tulsa, 93–120

Peters, K. E., Fraser, T. H., Amris, W., Rustanto, B., Hermanto, E., 1999. Geochemistry of Crude Oils from Eastern Indonesia 1. In AAPG Bulletin 83, 12.

Peters, K.E., Walters, C.C., Moldowan, J.M., 2005. The biomarker guide vol.2: biomarker and isotopes for petroleum exploration and earth history. Cambridge University Press, Cambridge.

Price, L.C., Barker, C.E., 1985. Suppression of vitrinite reflectance in amorphous rich kerogen-A major unrecognized problem. Journal of Petroleum Geology 8, 59–84. https://doi.org/10.1111/j.1747-5457.1985.tb00191.x.

Price, P.L., O'Sullivan, T., Alexander, R., 1987. The nature and occurrence of oil in Seram, Indonesia. Proceedings of Indonesian Petroleum Association 16th Annual Convention and Exhibition.

Rangel, A., P Parra, P., Niño, C., The La Luna formation: chemostratigraphy and organic facies in the Middle Magdalena Basin, Organic Geochemistry 31(12), 1267–1284, https://doi.org/10.1016/S0146-6380(00)00127-3.

Rojas, L. F., Quintero, P. Y., Carrillo, Z. H., 2016. Brittleness analysis: a methodology to identify sweet spots in shale gas reservoirs. Paper presented at SPE Argentina Exploration and Production of Unconventional Resources Symposium, Buenos Aires, Argentina. https://doi.org/10.2118/180955-MS

Rudyawan, A., Hall. R., 2012. Structural Reassessment of Banggai Sula Area: No Sorong Fault Zone. Proceedings, Indonesian Petroeum Association. Thirty-Sixth Annual Convention & Exhibition.

Rusmana, E., Sukarna, D., 1985. Tinjauan stratigrafi lengan tenggara Sulawesi dibandingkan dengan daerah sekitarnya. In Proceeding of Indonesian Associaton Geologist (IAGI), 14th Annual Convention (pp. 61–70).

Rusmana, E., Sukido, Sukarna, D., Haryanto, E., Simandjuntak, T. O., 1993. Geological map of the Lasusua -Kendari Quadrangles (Quadrangles 2112, 2212), Sulawesi, Scale 1:250,000. Geological Research and Development Centre.

Satyana, A. H., Irawan, C., Kurniawan, W. 2013. Revisit Geology and Geochemistry of Buton Asphalt Deposits, SE Sulawesi: Implications for Petroleum Exploration of Buton Area.

Sawada, K., 2006. Organic facies wand geochemical aspects in Neogene neritic sediments of the Takafu syncline area of Central Japan: Paleoenviromental and sedimentological reconstructions. Island Arc 15, 517–536. https://doi.org/10.1111/j.1440-1738.2006.00546.x.

Sawada, K., Handa, N., Shiraiwa, Y., Danbara, A., Montani, S., 1996. Long-chain alkenones and alkyl alkenoates in the coastal and pelagic sediments of the northwest North Pacific, with special reference to the reconstruction of Emiliania huxleyi and Gephyrocapsa oceanica ratios. Org. Geochem. 24, 751–764. https://doi.org/10.1016/S0146-6380(96)00087-3.

Schlumberger., 2005. Case Study: sCore lithofacies classification reveals Barnett shale reservoir quality. Schlumberger.

Selley, R.C. Sonnenberg, S.A., 2015. Elements of Petroleum Geology. 3rd Edition, Elsevier, Amsterdam, 507 p. https://doi.org/10.1016/C2010-0-67090-8

Serra, O., 1979. Diagraphies Différés base de l'interprétation. mémoire1 tome1. Services Techniques Schlumberger, Paris, pp 631.

Simandjuntak, T. O., Surono, Sukido., 1993. Geological Map of the Kolaka Sheet quadrangles 2111, 2210, 2211, Sulawesi, scale 1:250,000. Geological Research and Development Centre.

Simmons, K., 2023. Standard operating procedure (SOP) for sediment sampling. US Environmental Protection Agency.

Spakman, W., Hall, R., 2010. Surface deformation and slab-mantle interaction during Banda arc subduction rollback. Nature Geoscience 3(8), 562–566. https://doi.org/10.1038/ngeo917

Sprague, R. A., Melvin, J. A., Conradi, F. G., Pearce, T. J., Dix, M. A., Hill, S. D., & Canham, H., 2009. Integration of core-based chemostratigraphy and petrography of the Devonian Jauf Sandstones, Uthmaniya Area, Ghawar Field, Eastern Saudi Arabia. Search and Discovery Article 20065, 34.

Subroto, E.A., Alexander, R., Kagi, R.I., 1991. 30-norhopanes: their occurrence in sediments and crude oils. Chemical Geology 93, 179–192.

Surono., 1994. Stratigraphy of the Southeast Sulawesi continental terrane, eastern Indonesia. J. Geol. Miner. Resource. IV, 8–1.

Surono., 1998. Geology and origin of the SE Sulawesi continental terrane, Indonesia. Media Tek, 20, 13–31.

Surono, Bachri, S., 2002. Stratigraphy, sedimentation and palaeogeographic significance of the Triassic Meluhu Formation, Southeast arm of Sulawesi, Eastern Indonesia. Journal of Asian Earth Sciences 20(2), 177–192. https://doi.org/10.1016/s1367

Surono, Hatono, U., 2013. Geology of Sulawesi. Centre of Geological Survey, Ministry of Mineral and Energy Resources of Indonesia. LIPI Press, 352 p.

Taylor, S.R., McLennan, S.H., 1985. The Continental Crust: Its Composition and Evolution. Blackwell, Oxford, pp. 312.

Takahashi, G., 2015. Sample Preparation for X-Ray Fluorescenc Analysis III. Pressed and Loose Powder Methods. The Rigaku Journal 31(1), 26–30.

Taylor, G. H., Teichmüller, M.-Th., Davis, A., Diessel, C. F. K., Littke, R., Robert, P., 1998. Organic Petrology. Gebrüder Borntraeger, Berlin.

Tissot, B., & Welte, D. H. (1984). Petroleum formation and occurrence (pp. 699). Springer Science & Business Media.

Tobia, F. H., Al-Jaleel, H. S., Ahmad, I. N., 2019. Provenance and depositional environment of the Middle-Late Jurassic shales, northern Iraq. Goesciences Journal 23(5), 747–765.

Tobing, S. M., 2008. Aspal Buton dan Kajian Geokimia Hidrokarbon. Buletin Sumber Daya Geologi 3, 31–47.

Tucker, M.E., Calvet, F. and Hunt, D. (1993) Sequence Stratigraphy of Carbonate Ramps: System Tracts, Models and Application to the Muschelkalk Carbonate Platforms of Eastern Spain. In: Posamentier, H.W., Summerhayes, C.P., Haq, B.U. and Allen, G.P., Eds., Sequence Stratigraphy and Facies Associations, International Association of Sedimentary Special Publication 18, 397–415.

Tyson, R. V. (2005). The “productivity versus preservation” controversy: cause, flaws, and resolution. In Paleoceanography (pp. 157–175). Springer, Dordrecht.

Ulmer-Scholle, D. S., Scholle, P. A., Schieber, J., Raine, R. J., 2014. A color guide to the petrography of sandstones, siltstones, shales and associated rocks. AAPG Memoir 109.

Villeneuve, M., Cornée, J.-J., Gunawan, W., Martini, R., Tronchetti, G., Janin, M.-C., Saint Marc, P., & Zaninetti, L., 2001. La succession lithostratigraphique du bloc de Banda dans la region de Kolonodale (Sulawesi central, Indonesie). Bulletin de la Société géologique de France, 172, 59–68. https://doi.org/10.2113/172.1.59

Xianqing, L. Bo, X., Ningning, Z., Anlai, M., Tieguan, W., Aiyun, Z. , 2004. Organic petrological studies on immature source rocks. Chin. J. Geochem. 23, 15–25. https://doi.org/10.1007/BF02841132

Waples, D. W., 1985. Geochemistry in petroleum exploration. International Human Resources Development Corporation, Reidel Publishing Company, 31–180.

Wei, X., Zhang,K,. Li, Q., Hu, D., Wei, Z., Liu, R., Liu, Z., Liu, J., 2021. Quantitative characterization of pore space for the occurrence of continental shale oil in lithofacies of different types: Middle Jurassic Lianggaoshan Formation in Southeastern Sichuan Basin

of the Upper Yangtze Area. Geofluids, 2021 (1-18). https://doi.org/10.1155/2021/9906500

Wei W., Algeo, T. J., 2020. Elemental proxies for paleosalinity analysis of ancient shales and mudrocks. Geochimica et Cosmochimica Acta. Volume 287. 341–366. https://doi.org/10.1016/j.gca.2019.06.034.

Weltje, G.J. & von Eynatten, H., 2004. Quantitative provenance analysis of sediments: review and outlook. Sedimentary Geology, 171(1–4), pp.1–11.

Wilkin, R.T., Barnes, H.L., Brantley, S.L., 1996. The size distribution of framboidal pyrite in modern sediments: an indicator of redox conditions. Geochem. Cosmochim. Acta 60, 3897–3912.

Xia, L. W., Cao, J., Wang, M., Mi, J. L., Wang, T. T., 2019. A Review of Carbonates as Hydrocarbon Source Rocks: Basic Geochemistry and Oil–Gas Generation. Petroleum Science 16, 713–728.

Xiao, S., Yin, C., Liu, L., Gan, Y., Cao, R., & Wei, G. (2022). Relationship between mineralogy, organic matter abundance and preservation in marine source rocks. International Journal of Coal Geology 244, 103849

Yu, H., Yang, R., He, Z., Bao, H., Han, Y., Zhang, W., Xiong, S., Wang, F., Hu, Q., He, S., 2023. Full-scale pore structure and fractal characteristics of continental organic-rich shale: a case study of the Dongyuemiao Member of Jurassic Ziliujing Formation in the Fuxing area, Eastern Sichuan Basin. *Energy and Fuels 37* (14), 10426-10443. https://doi.org/10.1021/acs.energyfuels.3c01547

Zumberge, J. E., 1984. Source Rocks of the La Luna Formation (Upper Cretaceous) in the Middle Magdalena Valley, Colombia. AAPG Studies in Geology, 127–133.